Advanced Drug Delivery Reviews 143 (2019) 115–133

Contents lists available at ScienceDirect

Advanced Drug Delivery Reviews

journal homepage: www.elsevier.com/locate/addr

Hybrid drug nanocrystals

Yi Lu [a,b], Yongjiu Lv [b], Tonglei Li [a,*]

[a] Department of Industrial & Physical Pharmacy, College of Pharmacy, Purdue University, West Lafayette, IN 47907, USA
[b] Key Laboratory of Smart Drug Delivery of MOE, School of Pharmacy, Fudan University, Shanghai 201203, China

ARTICLE INFO

Article history:
Received 10 January 2019
Received in revised form 14 June 2019
Accepted 24 June 2019
Available online 26 June 2019

Keywords:
Hybrid nanocrystals
Fate
In vivo
Intracellular
AIE
ACQ
FRET

ABSTRACT

Nanocrystals show promise to deliver poorly water-soluble drugs to yield systemic exposure. However, our knowledge regarding the *in vivo* fate of nanocrystals is in its infancy, as nanocrystallization is simply viewed as an approach to enhance the dissolution of drug crystals. The dying crystal phenomenon inspired the development of hybrid nanocrystals by physically embedding fluorophores into the crystal lattice. This approach achieved concurrent therapy and bioimaging and is well-established to study pharmacokinetics and nanocrystal dissolution *in vivo*. Nanocrystals also offer the advantage of long-term durability in the body for interacting with biological tissues and cells. This review introduces the hybrid nanocrystal technique, including the theoretical concepts, preparation, and applications. We also discuss the latest development in self-discriminative hybrid nanocrystals utilizing environment-responsive probes. This review will stimulate further development and application of nanocrystal-based drug delivery systems for theranostic strategies.

Contents

Abbreviations: AIE, aggregation-induced emission; ACQ, aggregation-caused quenching; BBR, brilliant blue R; BODIPY, boron-dipyrromethene; CE, columnar epitheliums; CLSM, confocal laser scan microscope; CT, computerized tomographic scanning; F127-PTX-NCs, F127 physically coated paclitaxel nanocrystals; F68-PTX-NCs, F68 physically coated paclitaxel nanocrystals; FAE, follicular-associated epithelial cells; FA-PEG-Dp-PTX-NCs, folic acid chemically conjugated paclitaxel nanocrystals through polydopamine; FA-PEG-PTX-NCs, folic acid physically coated paclitaxel nanocrystals; FRET, Förster resonance energy transfer; GC, goblet cell; LP, lamina propria; MFI, median fluorescence intensity; MPS, mononuclear phagocytic system; NIR, near-infrared; PEG-Dp-PTX-NCs, PEG chemically conjugated paclitaxel nanocrystals through polydopamine; PEG-PTX-NCs, PEG physically coated paclitaxel nanocrystals; PK, pharmacokinetics; PPs, peyer's patches; PTX-NCs, paclitaxel nanocrystals; SBT, spectral bleed-through; SRB, sulforhodamine B; STEM, scanning transmission electron microscopy; TEM, transmission electron microscope; TPE, tetraphenylethene; WGA, wheat germ agglutinin.

* Corresponding author.
E-mail address: tonglei@purdue.edu (T. Li).

https://doi.org/10.1016/j.addr.2019.06.006
0169-409X/

1. Introduction

>70% of drug candidates produced by drug discovery approaches, including combinatorial chemistry and high-throughput screening, are highly lipophilic and intrinsically poorly soluble in water [1]. Poor aqueous solubility presents one major hurdle for drug development [2,3]. Particle size reduction becomes a viable alternative to deliver poorly soluble drugs. However, micronization has shown only limited improvement to enhance formulation performance [4–6]. Nanosizing shows more promise than micronization due to dramatically increased surface area [7] and larger curvature [8–10]. Suspensions of nanosized drug particles may be delivered *via* parenteral routes [11]. Since the pioneering work by Liversidge to prepare stable drug nanoparticles with sizes <400 nm [22], the drug nanocrystal formulation has gained much attention to deliver poorly soluble drugs. Nanocrystal preparation can use either top-down or bottom-up techniques [12,13]. To date, a dozen nanocrystal drug formulations are currently marketed for either parenteral or oral administration. Nevertheless, little is known about the *in vivo* outcome of a nanocrystal delivery system. This barrier arises from the inability to reliably and practically trace nanocrystals in the body, which limits developing this formulation technique further [14], especially for parenteral administration by the drug host.

Using guest inclusion, a well-known phenomenon in solid-state chemistry, we developed a hybrid nanocrystal for concurrent therapy and bioimaging by embedding imaging agents (*e.g.* fluorophore, radionucleotide, or contrasting agent) inside the crystal lattice [15]. After this innovative approach, a series of hybrid nanocrystal systems have been developed [16–20]. However, the fluorescent probes used in our earlier studies were static and not environment-sensitive, leading to indiscriminant imaging signals between trapped fluorophores in the nanocrystals and released fluorophores. So, we recently explored using environment-responsive probes to circumvent this limitation [21–23]. Both aggregation-induced emission (AIE) and aggregation-caused quenching (ACQ) fluorophores demonstrated significant potential to develop self-sensing hybrid nanocrystals. We speculate that *in vivo* transportation and dissolution kinetics of nanocrystals will emerge through using the hybrid nanocrystal technique.

This review begins with a brief recount of nanocrystal development and current studies examining the *in vivo* fate of nanocrystals. We then discuss concepts and applications of hybrid nanocrystals.

2. Nanocrystal development history

In a drug delivery system, depending on its solubility, stability, and delivering route, the drug may be formulated in the liquid or solid state. Normally, the solid state is either crystalline where drug molecules are self-assembled in regular, long-range ordered structures, or amorphous where such ordering is lacking and packing is random. Amorphous formulations have been investigated and utilized in drug products because of enhanced dissolution kinetics [24], but their propensity to physically transform into the crystalline state requires the use of polymeric additives (excipients) and also raises concerns of the inherent physical instability [25]. For delivering poorly soluble drugs, maintaining the crystalline state while keeping the particle size small has remained a practical and reliable approach. Nanocrystal is such a formulation strategy.

2.1. Nanocrystals as drug delivery system

Nanocrystals are crystalline drug particles with sizes generally smaller than 1 μm [26–31]. In some cases, surfactants and/or polymers are physically adsorbed on the surface of the nanocrystals to reduce particle aggregation. Doxil® may likely be the first nanocrystal formulation for injection, in which needle-like doxorubicin sulfate nanocrystals are loaded inside liposomes [32], although the original nanocrystal formation may have been accomplished unintentionally. Recently, the structural parameters of doxorubicin nanorods inside liposomes were reconstructed using the coherent diffraction imaging technique [33]. Nanocrystals circulating in the blood bear similar *in vivo* behaviors to conventional nanocarriers that are recognized and sequestered by mononuclear phagocytic system (MPS) cells. In turn, the MPS cells can act as depots to enhance the pharmacokinetics and biodistribution of delivered drugs [9,34]. Surface modification with hydrophilic polymers can enable nanocrystals to evade phagocytosis with prolonged circulation, facilitating accumulation in tumors [10,35–37]. Ligand modification by physical adsorption may enable nanocrystals to target cancer cells [38]. Because there are no carrier chemicals, a nanocrystal formulation may eliminate any toxicity initiated by the carrier excipients. This will yield drug loading as high as 100%, which will achieve satisfactory therapeutic outcomes at a low dose. One single dose of Ryanodex® (dantrolene sodium injectable nanosuspension), recently FDA-approved to treat malignant hyperthermia, provides sufficient treatment for most patients. In contrast, more than ten vials of traditional Dantrium® (20 mg/vial) are required to treat an adult patient [39].

Oral delivery of drug nanocrystals may be traced to the study by Liversidge et al. in 1992 [40]. The prepared danazol and steroid A nanocrystals by media milling showed 15.9- and 7.1-fold higher oral bioavailability than micronized counterparts, respectively [40,41]. To date, more than a dozen nanocrystal oral preparations exist and are approved for clinical use. Increased dissolution from nanosizing enhanced the bioavailability of these products [11,34,42]. In addition, nanocrystal formulations show improved dose proportionality, reduced fed/fasted variability and decreased inter-subject variability [43]. Nanocrystals have also been widely studied to enhance intravenous, transdermal, ocular and pulmonary deliveries of various drugs [10,44–47].

2.2. Preparation techniques

Nanocrystal preparation generally utilizes either a top-down or a bottom-up approach (Fig. 1) [13,46,48]. The top-down approach uses mechanical attrition, typically by media milling or high-pressure homogenization, to comminute coarse powders (top-down), while the bottom-up approach grows nanocrystals from solution (bottom-up) [49,50]. Comparatively, the top-down method is more adaptive [25] and flexible for production scale [24] than bottom-up. Although most commercial nanocrystal products are prepared through commination, the top-down technique is generally time- and energy- consuming [51]. Grinding does achieve the desired particle size and size distribution, although shedding of the grinding media into the product may cause unexpected and unintended side-effects [12,13]. Conversely, bottom-up techniques have some advantages. They are generally energy and time conservative, and they have superior control of the crystallinity and particle size distribution [49,50]. The bottom-up method uses anti-solvent crystallization. By mixing with a solvent in which the solute becomes poorly soluble (*i.e.*, anti-solvent), crystallization is induced because of supersaturation. Abrupt and simultaneous nucleation is an essential step to achieve small and uniform nanocrystals [13,52,53]. Techniques such as sonication [54–59], confined impinging jet [60–64], multiple inlet vortex mixing [65], and high-gravity controlled precipitation [66–68] are utilized to increase the mixing efficiency of the solutions. In some cases, rapid crystallization leads to the amorphous state or a less stable crystalline form, which permits even faster dissolution [25].

Ideally, the mixing process avoids nucleation, while the end of mixing induces abrupt and simultaneous nucleation. The local supersaturation formed at the interface of the two fluids during the mixing process may nevertheless trigger successive nucleation, which leads to larger and fewer crystals [53,69,70]. This outcome deteriorates in scale-up production. When nucleation is triggered directly from a metastable solution, homogeneous nuclei may be produced, which then leads to uniform nanocrystals. This idea arose to grow carrier-free paclitaxel nanocrystals with the particle size smaller than 250 nm and polydispersity index <0.25 by triggering nucleation from a paclitaxel metastable solution [52]. The crystallization efficiency is mostly limited by the metastable limit of the drug in solution.

3. Nanocrystal fate *In vivo*: current studies

3.1. Current approaches

Upon injection or ingestion, drug nanocrystals should dissolve to release drug molecules into the *in vivo* milieu. The nanocrystals themselves also interact with the blood, extracellular matrix, and various cell types. However, kinetic information on the *in vivo* processing of drug nanocrystals is limited, as most available pharmacokinetic and biodistribution data utilizes the measurement of overall drug concentrations. For specific pharmacokinetic and biodistribution data *via* i.v. injection, please refer to our recent reviews [12,13]. In practice, during biosample treatment, both intact nanocrystals and dissolved drug molecules are extracted for the analyses, leading to no specific data of nanocrystals in the samples. To obtain the actual behavior of nanocrystals, we must separate the intact particles from dissolved drugs through centrifugation or Sephadex column. Such a process itself may accelerate dissolving the nanocrystals. To the best of our knowledge, no workable approaches are currently available to dynamically differentiate drug nanocrystals from dissolved molecules *in vivo*.

Using TEM, studies observed crystalline particles in a biological sample in rat spleen macrophages and mesenteric lymph fluid following intravenous injection of itraconazole nanocrystals and duodenal administration of nimodipine nanocrystals, respectively (Fig. 2) [71,72]. Despite excellent resolution, TEM is quite limited, so detecting particle distribution at the whole body level is impossible. TEM only provides static viewing and lacks the capability for dynamic monitoring [73]. Moreover, TEM also requires special care in sample preparation to avoid recrystallization of drug molecules during dehydration.

Fluorescence-based whole-body imaging permits tracking translocation of nanoparticles *in vivo* [74–77]. The absence of carrier materials impedes labelling nanocrystals using the same approach as tagging nanocarriers. Autofluorescent drug molecules enable tracing nanocrystals. Transdermal transportation of curcumin nanocrystals

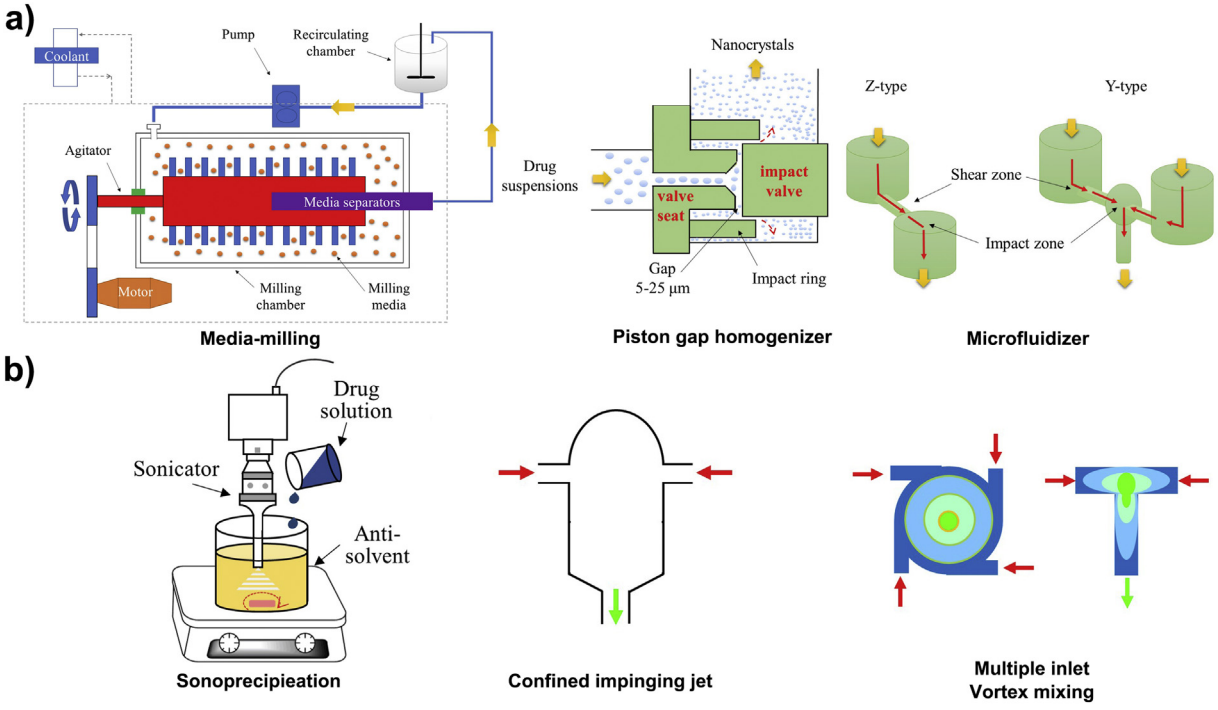

Fig. 1. Techniques employed towards preparing nanocrystals. (a) Top–down techniques in which coarse drug crystals are comminuted by high pressure or milling media. (b) Bottom–up techniques in which drug nanocrystals grow from solution. Images taken from [20] complying with the CC BY-NC-ND license (http://creativecommons.org/licenses/by-nc-nd/4.0/).

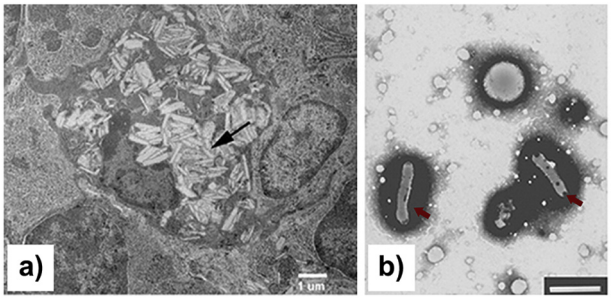

Fig. 2. Observation of crystalline particles in biological samples by TEM. Crystalline material found in rat (a) spleen macrophages following intravenous injection of itraconazole nanocrystals and (b) lymph fluid following duodenal administration of nimodipine nanocrystals. Images taken with permission from [71,72].

has been studied using confocal laser scanning microscopy [78]. Coumarin 6 revealed the transport mechanism of its nanocrystals through MDCK monolayers in larval zebrafish [79]. A hydrolyzable fluorescein diacetate was used to study the ocular penetration of its nanocrystals [80]. Unfortunately, only a limited number of therapeutic drugs are autofluorescent. Since each nanocrystal formulation exhibits distinct physicochemical properties, which impacts *in vivo* behavior, results acquired with a few model nanocrystals cannot be extrapolated to most other nanocrystals.

3.2. Exploring the in vivo fate of nanocrystals

The complexity of the *in vivo* environment requires diligence to elucidate the *in vivo* fate of nanocrystals. The most striking feature of nanocrystals is extremely high surface area, which significantly enhances the dissolution rate [81]. The apparent solubility of nanosized particles can be higher than bulk materials according to the Ostwald-Freundlich equation [10]. The dissolution of poorly soluble drugs can be dramatically enhanced through nanosizing, as supported by *in vitro* dissolution tests [8–10]. However, the *in vivo* environment is completely different from an *in vitro* test, which includes a limited volume of physiological fluid that nanocrystals contact upon ingestion and the absence of stirring processes. Thus, using *in vitro* tests remains insufficient or even misleading to understand the *in vivo* fate of nanocrystals.

We primarily do not know whether nanocrystals dissolve instantly or stay intact for a specific duration after i.v. injection. It is assumed that nanocrystals dissolve quickly in the blood to release the drug into systemic circulation. Oridonin nanocrystals of 103 nm in size showed a similar biodistribution to the solution after i.v. injection [82]. Although AZ68 amorphous nanosuspensions (100–150 nm) showed enhanced solubility and dissolution rate compared with crystalline particles (300–400 nm), both formulations showed similar pharmacokinetic profiles after i.v. administration [83].

Some argue that nanocrystals in the blood may survive blood circulation for recognition and ingestion by phagocytic cells [12,13]. Rabinow et al. provided proof of MPS deposition of itraconazole nanocrystals *via* i.v. injection (Fig. 2a) [71]. Transport by phagocytic cells altered nanocrystal biodistribution, which led to significant accumulation in MPS cell-abundant organs, including liver, spleen and lung compared with the solution formulation [84–87]. In this instance, nanocrystals would dissolve slowly inside the phagocytic cells with the released drug molecules diffusing out of the cells, which could possibly improve pharmacokinetics, such as lower C_{max}, longer $t_{1/2}$ and better tolerance at higher doses [13]. We developed and tested camptothecin nanocrystals [88,89]. These injected nanocrystals did show longer $t_{1/2}$ and lower AUC than the camptothecin salt solution in tumor-bearing mice. This result supports the MPS deposition hypothesis.

For the oral route, dissolution of a delivery system precedes absorption of drug molecules. It is generally assumed that nanocrystals of a poorly soluble drug dissolve much faster than bulk material or micronized particles upon ingestion [14]. The dissolved drug molecules permeate across biomembranes, facilitated by the resulting concentration gradient [14]. Along with other important physiological parameters such as pH, bile salts, gastric emptying rate, and motility, water content in the gastrointestinal tract has the potential to influence greatly the rate and extent of drug dissolution and, subsequently, drug absorption and systemic exposure [90,91]. Impact of the volume of intestinal water on the absorption and PK profiles of four poorly soluble drugs was investigated by compartment-based PK modeling [92]. Water content in the gastrointestinal tract is highly variable depending on the fasted/fed state and/or physiological/pathological conditions. One study in human volunteers [90] demonstrated the volume of gastric water declined rapidly to baseline (35 mL) with the emptying half-life of 13 min after ingesting 240 mL water in the fasted state, while the total intestinal water volume was around 77 mL distributed into 16 pockets of about 5 mL each. Given that nanocrystals may not dissolve instantaneously upon oral administration, it is possible that nanocrystals greatly interact with biological tissues including the epithelial membrane. In rats, nimodipine nanocrystals spread to the mesenteric lymph fluid following duodenal administration, suggesting absorption of some nanocrystals through the GIT membrane (Fig. 2b) [72].

Even with the few initial studies, the *in vivo* fate of nanocrystals remains unclear. Major difficulty to elucidate the underlying factors stems from reliable means to detect the dynamic dissolution process of nanocrystals in the biological environment and, more importantly, clearly distinguish nanocrystals from the dissolved drug molecules. Nanocrystals of different drugs could behave drastically from another, which impedes extrapolating data obtained from one type of nanocrystal to other drug nanocrystals.

4. The hybrid nanocrystal

4.1. Conception of hybrid nanocrystals

The well-known phenomenon of guest inclusions in solid-state chemistry inspired the idea of hybrid nanocrystals [15,93,94]. Bulk properties of a host crystal, such as optical appearance, mechanical durability, and electronic conductivity, can be significantly altered by including a minute amount of guests in the lattice of the host. Examples of guests or doped crystals include colored diamonds, synthetic alloys, and p- and n-type semiconductors. The colour of a diamond becomes drastically different due to the presence of some guest molecules, albeit only a trace amount. For example, the blue diamond arises from boron inclusion, while yellow due to nitrogen. The alloying elements are critical to improve the hardness, toughness, ductility, and other desired properties of a base metal. Increasing the carbon content in steel (the iron-carbon alloy) up to 2% leads to higher strength and toughness than iron. For semiconductors, doping a small amount of pentavalent or trivalent atoms can increase the conductivity of silicon. The retaining ability for the guest by the host generally depends on the interaction between the crystal and the included substance, as well as the rate of crystallization. Inclusion is generally enhanced by fast growth of a crystal host. Due to the limited amount of entrapped guest materials, the structure and integrity of the host crystal remain largely unaffected. Because guest molecules (or atoms) are embedded in the defect sites, guests of varying size reside in host crystals [95]. Although inclusion of biopolymers (*e.g.* proteins, oligonucleotides and dextrans) was attempted by crystals of phthalic acid and lactose monohydrate [96], the hosting capacity of these biopolymers is extremely low (0.1% to 0.01%). For bioimaging purposes, inclusion of a trace amount of imaging agents in a drug host does seem possible. Dye inclusion crystals have been studied for over a century, see Kahr et al. [94] for a comprehensive review. The distribution of dye molecules, may reveal better crystal growth mechanisms. For instance, a recent study of incorporating fluorophores in

calcite crystals illustrates mechanisms of biomineralisation [97,98]. They demonstrated that brilliant blue R (BBR) preferential binds to the acute step edges of calcite crystals.

Inspired by dying crystals, our group developed drug nanocrystals that integrate fluorophores to achieve concurrent disease treatment and bioimaging in real-time and *in situ* [16–20]. The idea of so-called hybrid nanocrystal is illustrated in Fig. 3 a. A hybrid nanocrystal system may be composed of a drug, an imaging agent, a ligand, and or biocompatible polymer. To achieve a therapeutic effect, the drug also serves as the crystal host for guest molecules. Imaging agents may include fluorophores, radionucleotides, and contrast metals. As proof of principle, we added fluorescein and rhodamine during the growth of aspirin and acetaminophen crystals, respectively, and obtained crystals showing fluorescence (Fig. 3b). In addition to organic fluorescent molecules, we embedded inorganic gold atoms/ions in camptothecin nanocrystals [20]. Transmission electron microscope (TEM) and scanning transmission electron microscopy (STEM) images clearly show that gold clusters were incorporated into the camptothecin nanocrystals (Fig. 3c). Due to gold's high attenuation coefficient, these nanocrystals may be used for computerized tomographic scanning (CT) imaging and cancer treatment. Ligands and/or polymers may be either stoichiometrically integrated to form cocrystals or entrapped as defects. When presented on the crystal surface, ligands and/or polymers could facilitate targeted drug delivery through receptor-mediated endocytosis and/or tumor accumulation by enhancing blood circulation.

4.2. Development of hybrid nanocrystals

Using paclitaxel as the host crystal, we have developed and tested a hybrid nanocrystal system in our laboratory [16–19]. We tested several fluorophores for inclusion, which showed little effect on the size, morphology, or crystallinity of the paclitaxel nanocrystals (Fig. 4). The samples in Fig. 5c illustrate that the fluorescence seen from the nanocrystal suspensions was truly emitted by the fluorophores embedded in the paclitaxel nanocrystals, not from the released dye molecules whose amount was minimal. Due to the extremely low solubility of paclitaxel (*ca.* 0.2 μg/mL), we estimated a 0.86% entrapment ratio would release <0.002 μg/mL free fluorescein molecules. We observed no fluorescence from the dye solution from this concentration (Fig. 4c). Interestingly, decreasing the amount of incorporated fluorescin caused the fluorescence emission to shift from green to blue, while the pure dye solution remained unchanged (Fig. 4c). We conclude such a phenomenon could result from the excited state of the dye acting on the local environment of the crystal.

Near-infrared (NIR) fluorophores, such as FPR-749, have been integrated in drug nanocrystals for bioimaging. Exploiting the strong tissue penetrance of NIR fluorescence coupled with less interference from biological autofluorescence, NIR fluorophores provide non-invasive and real-time tracking of nanocrystals *in vivo* [19]. We demonstrated that mice upon tail-vein injection of hybrid nanocrystals with FPR-749 showed strong fluorescence at 780 nm (Fig. 4d

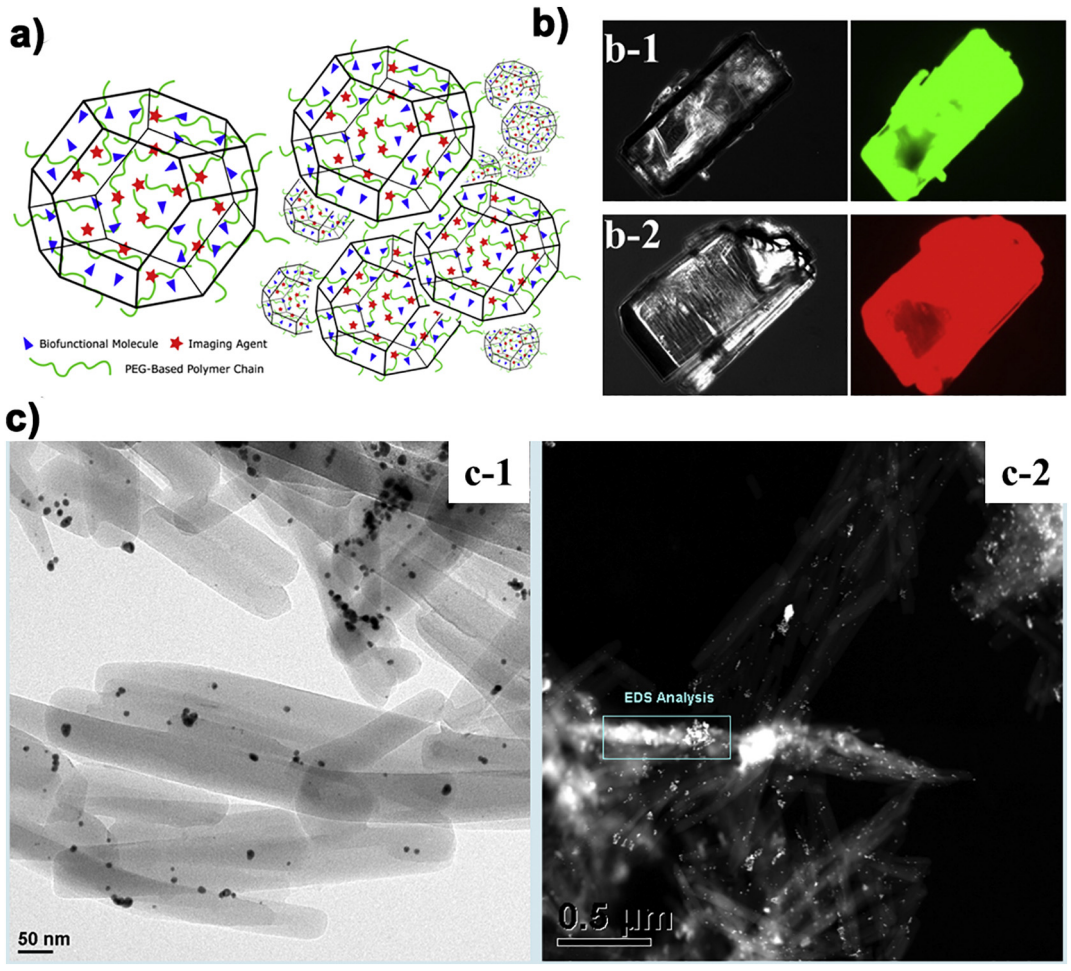

Fig. 3. Hybrid nanocrystal. (a) Illustration of a hybrid nanocrystal system using a drug as the host, and imaging agents, ligands, and biocompatible polymers as the guest. (b) Hybrid crystals of aspirin (b-1) and acetaminophen (b-2) with fluorescein and rhodamine emitting green and red fluorescence, respectively. (c) TEM (c-1) and STEM (c-2) images of camptothecin/gold hybrid nanocrystals showing gold clusters inside the crystal. Images taken from [20] complying with the CC BY-NC-ND license (http://creativecommons.org/licenses/by-nc-nd/4.0/).

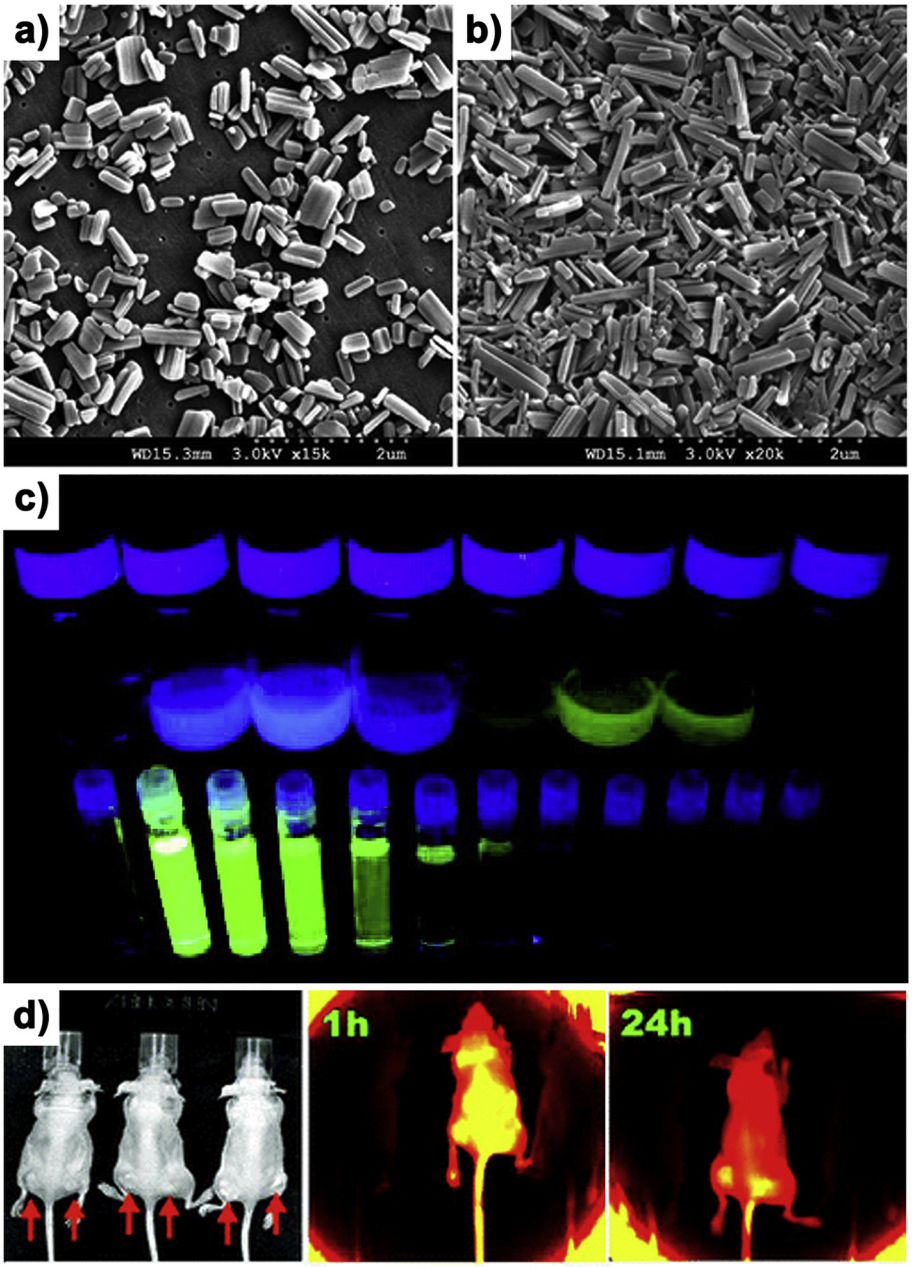

Fig. 4. Characterization of hybrid paclitaxel nanocrystals developed in our laboratory. (a) Scanning electron micrographs of pure paclitaxel nanocrystals and (b) hybrid paclitaxel nanocrystals. (c) Suspensions of hybrid paclitaxel nanocrystals with fluorescein under UV light. Back row (left to right): pure solvent, 0.015, 0.028, 0.022, 0.25, 0.83, and 0.86% dye in hybrid nanocrystals, and pure paclitaxel nanocrystals. Front row (left to right): samples of pure dye solutions (4, 2, 1, 0.5, 0.25, 0.125, 0.0625, 0.031, 0.008, 0.002, 0.0005 μg/mL) and water. (d) Bright field and whole-body fluorescence imaging of tumor-bearing mice taken at 780 nm (mice from left to right given pure paclitaxel nanocrystals, hybrid paclitaxel nanocrystals with FPR-749 (an NIR dye), and rhodamine B, respectively; arrows indicate tumor sites). Images taken with permission from [16,18].

middle). Pure nanocrystals (Fig. 4d left) and hybrid nanocrystals with rhodamine B (Fig. 4d right) were also injected as controls, which emitted negligible fluorescence at 780 nm. Accumulation of hybrid nanocrystals at tumor sites could still be observed 24 h post injection (Fig. 4d). However, hybrid nanocrystals with fluorescein and rhodamine B exhibit strong interference from autofluorescence. While they are not optimal for animal imaging, these fluorophores can be used to study cellular interactions by confocal laser scan microscopy (CLSM).

Since our first publication in 2011, two generations of hybrid fluorescent nanocrystals have been developed (Table 1). Traditional fluorophors were adopted in the first generation of hybrid nanocrystals. In addition to water soluble fluorophors, poorly soluble ones, such as DiD, DiR, Cy5 and ethyl rhodamine B, were also tested. Environment-responsive fluorophores are used in second generation hybrid nanocrystals including tetraphenylethene (TPE) a typical AIE fluorophor; P2/P4 bears sensitive ACQ effects; and DiO and DiI compose Förster resonance energy transfer (FRET) pairs. The environment-responsive probes can enable self-discrimination of hybrid nanocrystals, which will be introduced in detail in the following sections. While paclitaxel is the first and most studied compound, other crystals, such as itraconazole, lapatinib, saquinavir, cyclosporine A, quercetin, and schisantherin A, have also been tested. The hybrid fluorescent nanocrystals provide a universal technique to track the distribution, transepithelia transportation and intracellular fate of nanocrystals.

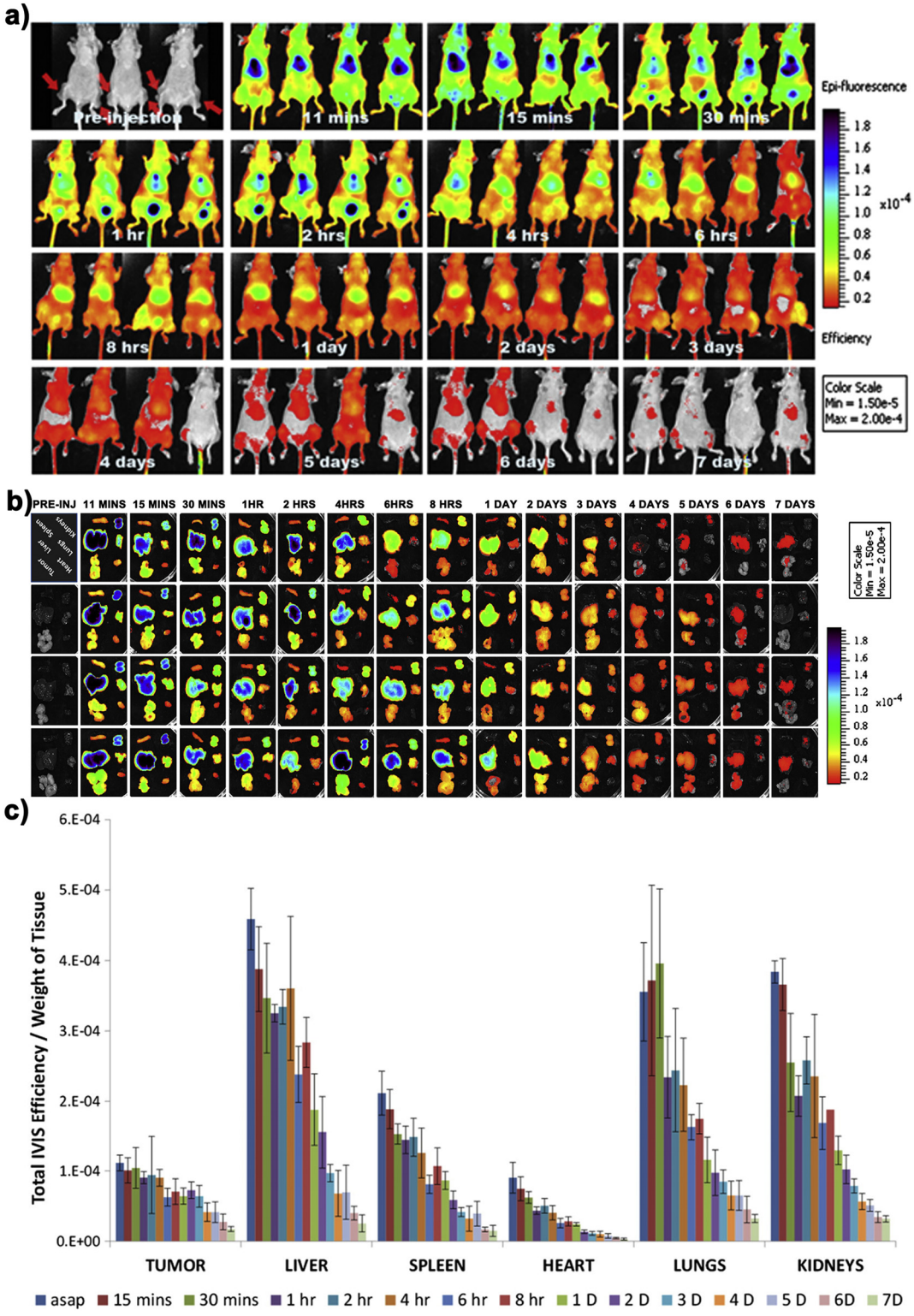

Fig. 5. Biodistribution of paclitaxel hybrid nanocrystals with FPI-749 *via* i.v. injection. (a) IVIS images of tumor-bearing mice following intravenous administration. (b) IVIS images of *ex-vivo* tissues over time. (c) The fluorescence distribution (total IVIS efficiency per weight of tissue) in tumor and major tissues over time. Images adapted with permission from [16].

4.3. Preparation of hybrid nanocrystals

Formation of hybrid nanocrystals generally requires a bottom-up process of crystallization, specifically using the antisolvent precipitation method (Table 1). With imaging agents in the growth media, incorporating the guest in defect sites in the crystal lattice of the host is realized during growing of host crystals. Through the process, imaging agents can be solubilized in the solvent or antisolvent, depending on its lipophilicity or hydrophilicity. Hydrophilic fluorophores, such as FPR-749, fluorescein and rhodamine B, are dissolved in water, which serve as antisolvent. Lipophilic dyes, such as DiD, DiR, Cy5 and P2, are dissolved in the organic phase, in which the drug is likely dissolved. To generate paclitaxel hybrid nanocrystals with FPR-749 fluorophore [18], the preparation process first dissolves FPR-749 in deionized water to a

Table 1
Summary of hybrid nanocrystals.

Drug	Imaging agents	λex/λem (nm)	Loading (%)	Application	Ref.
Paclitaxel	FPR-749	749/782	0.79	Distribution *via* i.v. injection	[18]
	Fluorescein	494/521	0.86		
	Rhodamine B	530/590	1.26		
Paclitaxel	FPR-648	648/672	0.01	Distribution *via* i.v. injection	[17]
Paclitaxel	FPI-749	750/782	/	Distribution *via* i.v. injection	[16]
Itraconazole	Ethyl rhodamine B	/	/	Cellular study, transepithelia transportation *via* oral route	[99]
Paclitaxel	DiR	748/780	/	Intratumoral residue and distribution	[100]
Paclitaxel	DiD	644/665	/	Intratumoral residue	[101]
Lapatinib	DiR	748/780	/		
Paclitaxel[a]	Cy5	646/662	/	Cellular uptake and *in vivo* distribution *via* i.v. injection	[102]
Saquinavir	Ethyl Rhodamine B	/	/	Cellular uptake, transepithelia transportation *via* oral route	[103]
Paclitaxel	TPE	/	2.2	Intracellular fate	[21]
Cyclosporine A	P2	708/732	0.05	Transepithelia transportation and biodistribution *via* oral route	[22]
	P4	651/662	0.03	Cellular uptake and transportation	
Quercetin	P2	708/732	0.01	Transepithelia transportation and biodistribution *via* oral route	[23]
	P4	651/662	0.02	Cellular uptake and transportation	
Schisantherin A	DiO/DiI	/	/	Intracellular fate	[104]
Camptothecin	gold	/	/	/	[20]

[a] Nanocrystals prepared by freeze-drying of frozen emulsion. The rests all prepared by antisolvent precipitation.

concentration of 5 mg/mL, followed by mixing with a paclitaxel ethanol solution (5 mg/mL) under mechanical stirring at 1000 rpm. Any loosely bound dyes on the crystal surface of paclitaxel crystals are removed by several water rinses.

Freeze-drying of an emulsion solution was employed to prepare hybrid paclitaxel nanocrystals with Cy5 [102]. In this study, paclitaxel and Cy5 were dissolved in 100 μL dichloromethane, which was mixed with 10 mL Pluronic F127 aqueous solution to form an oil-in-water emulsion under supersonic vibration. The emulsion was immersed in liquid nitrogen and frozen instantaneously. Paclitaxel hybrid nanocrystals were then yielded by freeze drying the frozen emulsion. By adjusting the paclitaxel concentration in the oil phase and the supersonic vibration intensity, 10 nm and 70 nm hybrid nanocrystals were obtained.

Because fluorophore molecules are integrated at the defect sites in the nanocrystal host, loading of the fluorophores is generally low (Table 1). The integration is on average <0.1%. Different fluorophores vary in their loading in same drug crystals. For example, loading ratios of fluorescein, rhodamine B, and FPR-749 in paclitaxel nanocrystals are 0.86%, 1.26%, and 0.79%, respectively [18]. The difference stems from variations in the molecular properties, such as molecular size and hydrophilicity/lipophilicity. Nonetheless, hybrid nanocrystals show similar particle sizes, morphology, and crystallinity to pure nanocrystals due to the limited loading of the fluorophores.

4.4. In vivo fate of hybrid nanocrystals

The current hybrid nanocrystal strategy cannot ensure exclusive imaging of nanocrystals *in vivo*. The dyes in the crystals, as well as the dye released when the crystals start to dissolve, contributes to the fluorescence signal. As the hybrid nanocrystals become more dissolved in the body, the fluorescence from the released dyes becomes more dominate. Thus, tracing the fluorescence *in vivo* cannot reveal the complex behavior of drug nanocrystals.

In order to accurately track the transport and dissolution of nanocrystals, the fluorescent signal must respond to the crystalline environment. In the first generation of hybrid nanocrystals, the fluorophores emit fluorescence irrespective of being embedded inside the nanocrystals or released as free molecules. Hybrid nanocrystals are incapable of discriminating themselves from the biological milieu from which the fluorophores are released [17,21]. The observed signals include emissions from the intact nanocrystals and the free probes. Along with the dissolution of nanocrystals, more probes are released and the signal intensity largely represents the quantities of the probe molecules. Since pharmacokinetics of free dyes are different from drug molecules or nanocrystals, discrepancy in the biodistribution between the fluorescence signals (dye molecules) and the drug begins to increase [17,21]. Thus, it is essential to choose a fluorophore that only lights up the hybrid nanocrystals. For this purpose, the environment-responsive fluorophores were utilized to make the second-generation hybrid nanocrystals. AIE, ACQ and FRET probes were adopted in parallel to prepare hybrid nanocrystals that are self-discriminative [21–23,104].

5. *In vitro* and *In vivo* studies using first-generation hybrid nanocrystals

5.1. In vivo distribution

Contrary to the belief of instant dissolution, nanocrystals may remain largely intact in blood circulation and reach various organs and tissues. Like any other nanoparticle-based delivery systems, drug nanocrystals can strongly interact with immune cells upon being administered, including macrophages and monocytes, most likely being taken up by these cells. It is no surprise that drug nanocrystals are distributed to organs of mononuclear phagocytic system (MPS), including liver, spleen, lung, and kidney. Besides, MPS influences disposition, clearance, efficacy, and toxicity of nanocrystals [105]. Understanding the interactions between nanocrystals and the MPS is essential to develop efficient and safe nanocrystal preparations as well as to provide more realistic predictions of the efficacy of nanocrystal-based therapies [105].Nanocrystals can also interact with proteins in the blood such as albumin. The protein-decorated surface of drug nanocrystals may significantly alter the tissue distribution and pharmacokinetics [106]. Adding to the complexity of the *in vivo* fate, dissolution of drug nanocrystals and constantly release of drug molecules occur concurrently with the transport of the nanocrystals. Thus, integrating imaging probes in drug nanocrystals potentially bring to light the various facets of *in vivo* behaviors.

Whole-body fluorescence imaging by IVIS tracked the translocation of paclitaxel hybrid nanocrystals with FPI-749 in tumor-bearing mice administered intravenously [16]. Strong peripheral fluorescence intensities emerged within the first few hours after injection. The fluorescence contrast between the tumor and peripheral areas began increasing after 1 h, which indicates the accumulation of nanocrystals at the tumor site (Fig. 5a). The overall intensity of the tumor remained distinct after 1 day and decreased after 5 days. Nonetheless, the strongest signals came from the liver area within a few minutes of injection and remained strong throughout the observation period. The tumor and major organs were excised and imaged under IVIS, and the total

fluorescence intensities from the individual tissues were normalized by the respective weights (Fig. 5b and c). The liver emitted the strongest intensities (normalized) with strong fluorescent signals also observed in the spleen and lungs. However, discrepancies occurred between the drug biodistribution measured by scintillation counting of ^{3}H-PTX that was spiked into the crystals and the fluorescence measurement and became more disparate over time. The likely reason is the undiscriminating capability of FPI-749 discussed above. Concerning drug accumulation, nanocrystals showed similar tumor accumulations to Taxol (the solubilized, micellar paclitaxel formulation). Even though tumor accumulation was low (<1%), both formulations exhibited tumor suppression effects. The toxicities by the nanocrystals, however, were significantly reduced. We propose these reduction stems from the absence of the toxic surfactant (cremophore) used in Taxol. Thus, high doses of nanocrystals may be administered. After the high dose accumulates in tissues, the nanocrystals can act as drug depots and release drug molecules back to systematic circulation.

5.2. Cellular uptake

Animal studies demonstrate that drug nanocrystals are capable of eliciting similar and better anticancer efficacies compared with the solubilized and encapsulated formulations of the drug. Cellular uptake mechanisms of nanocrystals, however, remain unexplored. It is possible that nanocrystals can undergo direct uptake by cells through endocytosis, or they can dissolve and release drug molecules that diffuse passively across the cell membrane. Both mechanisms may occur simultaneously. Sulforhodamine B (SRB) was physically integrated in paclitaxel nanocrystals to study cellular uptake mechanisms [19]. Due to the anionic state in the media, free SRB molecules could not be taken up significantly by KB cells. Conversely, significant SRB intensities were observed intracellularly, especially when concentration of the hybrid nanocrystals in the culture medium exceeded 25 μg/mL (Fig. 6 a). The results imply that nanocrystals were directly taken up by the KB cells. Importantly, the SRB signals were co-localized with Lyso-tracker signals, which indicates lysosomal cellular uptake of nanocrystals *via* endocytosis.Moreover, concentration measurements indicated that <0.5% of Taxol was taken up by the cells, which kept constant as incubation prolonged. The majority of the drug remained solubilized by cremophore in the culture media. On the other hand, the intracellular concentration of paclitaxel for nanocrystals increased from 15% at 0.5 h to >66% at 3 h of incubation, while the total extracellular drug concentration decreased accordingly. The extracellular solubilized drug concentration remained constant around 1.5%, likely due to the solubilization equilibrium with the nanocrystals in the media. Increased drug dose promoted cellular uptake of nanocrystals, but showed no significant influence by Taxol. Cellular uptake results confirmed endocytotic uptake of paclitaxel nanocrystals.

Surface-coated paclitaxel nanocrystals by surfactants showed similar cell uptake results to untreated ones under confocal laser scan microscopy (Fig. 6a). Still, polymer treatment exhibited considerably reduced cellular uptake (Fig. 6b). Interestingly, folic acid modification, whether physically coated or chemically conjugated to the polydopamine nanocrystal coating, showed no enhanced cellular uptake, despite KB cells overexpressing folate receptors. We suspect that insufficient folic acid moieties may be exposed on the crystal surface, whether *via* the surface conjugation or physical integration to the drug crystals. However, physical coating of folic acid-conjugated polymers on the nanocrystals enhanced drug internalization compared with folic acid chemically conjugated nanocrystals. In addition, Pluronic F68 seemed to promote additional crystal uptake relative to Pluronic F127-coated, as well as untreated systems. We found no clear trend in the cellular uptake affected by polymer treatment. Nonetheless, nanocrystal formulations showed much more potency than conventional, solubilized formulations in treating tumor cells. Nanocrystals taken up by cells led to more drugs inside the cells. The internalized nanocrystals dissolve slowly, generating a more lethality, which may be difficult to achieve through solubilized delivery systems *via* passive diffusion across the cell membrane. Further, undissolved nanocrystals may be recycled by other cells.

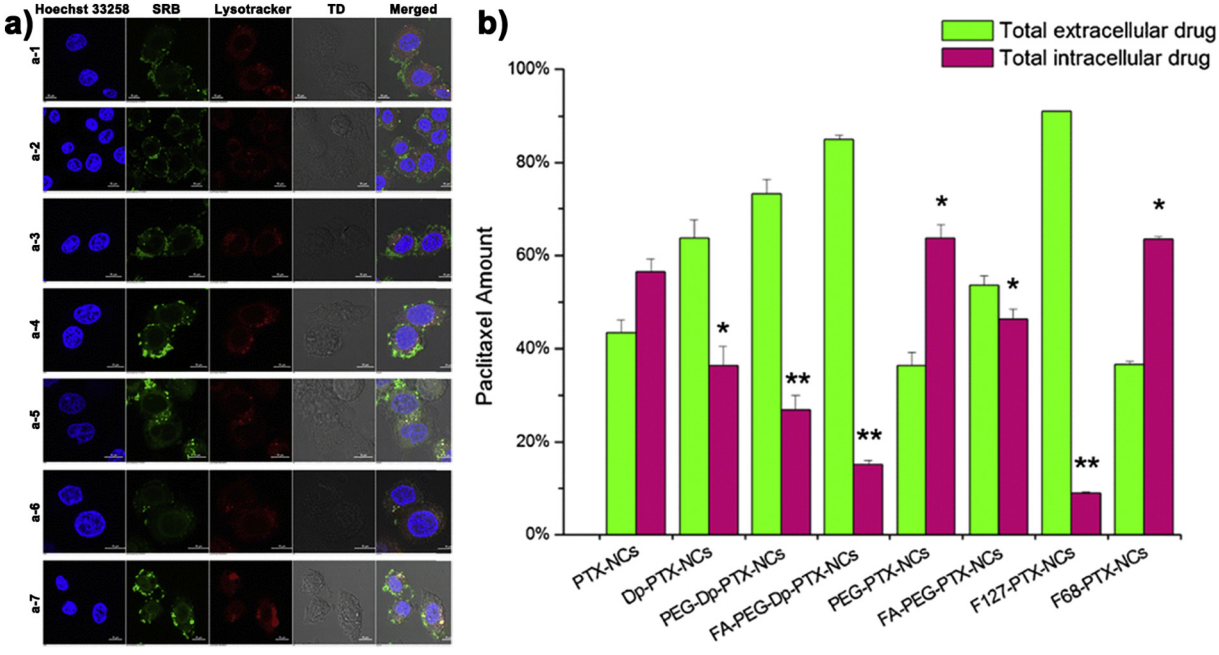

Fig. 6. Cellular uptake of paclitaxel nanocrystals at 3 h of incubation with KB cells. (a) Confocal images and (b) measurement of extracellular and intracellular drug amount. Blue and red indicates nuclei and lysosomes, respectively. Green indicated SRB. * and ** denotes significant ($P < .05$) and extremely significant ($P < .01$) difference between the marked group and pure nanocrystal group, respectively. a-1 pure paclitaxel nanocrystals (PTX-NCs), a-2 PEG chemically conjugated PTX-NCs through polydopamine (PEG-Dp-PTX-NCs), a-3 folic acid chemically conjugated PTX-NCs through polydopamine (FA-PEG-Dp-PTX-NCs), a-4 PEG physically coated PTX-NCs (PEG-PTX-NCs), a-5 folic acid physically coated PTX-NCs (FA-PEG-PTX-NCs), a-6 F127 physically coated PTX-NCs (F127-PTX-NCs), and a-7 F68 physically coated PTX-NCs (F68-PTX-NCs). Images taken with permission from [19].

5.3. Transport of hybrid nanocrystals through the GI membrane

To avoid shedding of surface modifiers, poly(acrylic acid)-b-poly (methyl acrylate) was covalently cross-linked on the surface of itraconazole nanocrystals to form a cage, where wheat germ agglutinin (WGA) was anchored by covalent conjugation [99]. Dual fluorescent labeling identified nanocrystals with ethyl rhodamine B (red) physically embedded inside the itraconazole nanocrystals and 5-aminofluorescein (green) chemically conjugated to the cage. Upon oral administration of the nanocrystals to rats, the intestinal tracts were removed and sectioned for examination under CLSM. Colocalization of both fluorescence signals in the lamina propria was observed, indicating absorption of drug nanocrystals (Fig. 7 a). However, the fluorescent signal of nanocrystals in the lamina propria was weaker than that on the apical side of the columnar epithelia, indicating faster dissolution of the nanocrystals in the lamina propria than outside the villi. The cross-membrane of nanocrystals was facilitated by endocytosis by goblet cells which are flask-shaped with a nucleus at the basal pole (Fig. 7b), doubly stained by WGA-Alexa Fluor 647 and UEA-I FITC (Fig. 7c).

6. Studies with second-generation hybrid nanocrystals

In order to fully understand the *in vivo* performance of drug nanocrystals, it is critical to isolate and distinguish fluorescent signals from embedded and released nanocrystals [107]. Environment-responsive probes present a solution. They enable nanocrystal fluorescence only when the probe is integrated (Fig. 8). Fluorescence is quenched or emitted at different wavelengths, which permits evaluating kinetics of intact nanocrystals. The change in fluorescence is spontaneous upon destruction of hybrid nanocrystals. Environmental factors that cause quenching or shifting of the fluorescence include hydrophilicity, hydrophobicity, and presence of water or quencher in the vicinity. The following sections discuss the use of second-generation hybrid nanocrystals that embed aggregation-induced emission, aggregation-caused quenching and Förster resonance energy transfer probes.

6.1. AIE fluorescent probe

6.1.1. Mechanism

AIE indicates fluorescence emission due to chromophore aggregation of probe molecules [108]. The fluorescence of such a probe is turned on when their molecular mobility is restrained, such as in an aggregated state or embedded in the matrix of nanoparticles [109]. As such, the loaded AIE probes illuminate nanoparticles, whereas released probes disperse in the environment and remain quenched.

One of the most used AIE probes is TPE. The TPE molecule has four aromatic rings conjugated together *via* a rigid ethylene (Fig. 9a). When dissolved in a solvent such as ethanol, the aromatic groups rotate/twist freely alongside the C—C bonds, exhibiting no fluorescence, as the excitation decays thermally. After adding water to the ethanol solution, TPE precipitates, which restricts the molecular motion in the precipitates. Importantly, dissipation of the excited state only occurs through photon emission (Fig. 9a, b). TPE-integrated nanocrystals

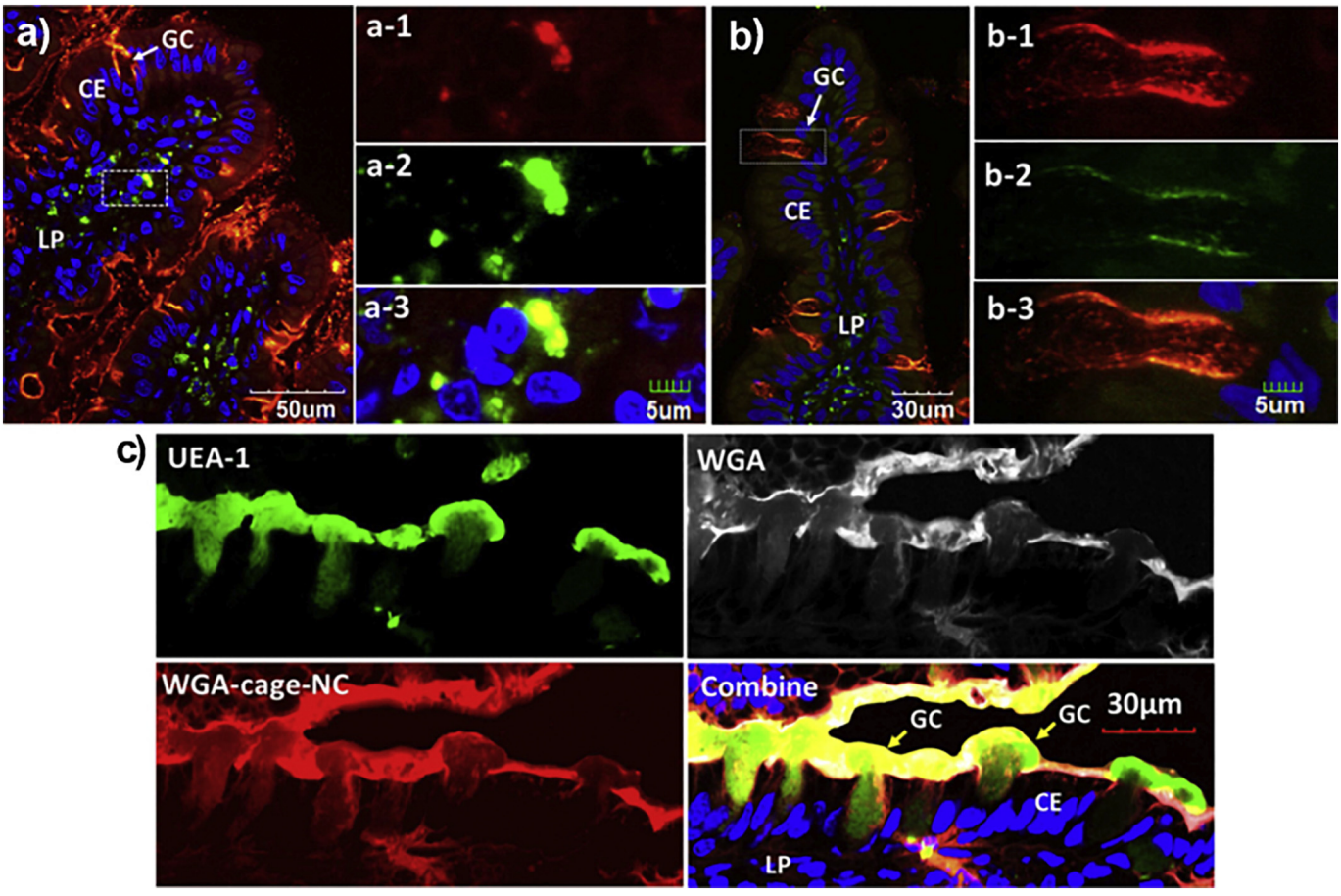

Fig. 7. Absorption of WGA anchored itraconazole nanocrystals. (a) Transepithelial transportation of intact WGA anchored nanocrystals to lamina propria (LP) of intestinal villi, confirmed by the (a-3) good colocalization of (a-1) red (nanocrystal core) and (a-2) green spots (cage). (b) Endocytosis of intact nanocrystals in goblet cell (GC); (b-3) good colocalization of (b-1) red (crystal core) and (b-2) green (cage) fluorescence spots indicates intact nanocrystals. (c) Doubly stained cells by UEA-I (green) and WGA-Alexa Fluor 647 (gray) are GCs, while single stained cells by WGA-Alexa Fluor 647 are villous columnar epitheliums (CE). WGA anchored nanocrystals (red) are preferentially taken up by GCs. Image taken with permission from [99].

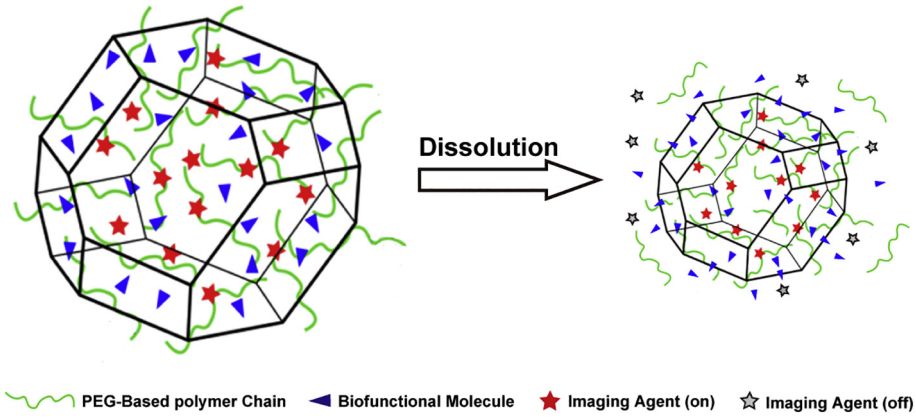

Fig. 8. Illustration of self-discriminative hybrid nanocrystals that embed environment-responsive fluorophores.

show similar AIE behavior. The hybrid nanocrystals emit fluorescence, while fluorescence diminishes when nanocrystals dissolve to release both the drug and probe molecules to the medium (Fig. 9c). The fluorescence intensity is quantitatively related to the amount of dissolved nanocrystals (Fig. 9d), enabling measurement of cellular uptake kinetics and intracellular dissolution of nanocrystals.

6.1.2. Study of intracellular fate of hybrid nanocrystals

Cell uptake studies measured hybrid paclitaxel nanocrystals with TPE [21]. Both KB and HT-29 cells incubated with the nanocrystals displayed visible blue fluorescence, characteristic of TPE. Imaging suggests that true paclitaxel nanocrystals and F68 coated nanocrystals were internalized into the cells (Fig. 10). The F68 coating visually showed little enhancement of uptake by KB cells, but considerable increase by HT-29 cells. The authors concluded stronger interactions between F68 and HT-29 membrane underlay the enhanced endocytosis. Moreover, after 3 h of incubation with the hybrid nanocrystals, the cells were removed and re-incubated in fresh culture medium for 2, 8, and 24 h, respectively. Confocal images of the cells showed decreased TPE fluorescence, more drastically in KB than HT-29, indicating dissolution (and possible exocytosis) of the nanocrystals. The difference between the two cell lines likely arose from the respectively intracellular environments. Quantification with flow cytometry supports the qualitative results obtained from CLSM. It is estimated that 20%–50% of internalized paclitaxel nanocrystals remain crystalline, depending on the cell type and dosage. Using flow cytometry, a decrease in median fluorescence intensity (MFI) was observed when cells were washed and re-incubated in fresh culture medium, indicating dissolution of the nanocrystals inside the cells. Moreover, the polymer surface coating could impede crystal dissolution, as dissolution was slower in HT-29 than KB cells.

6.2. ACQ fluorescent probes

6.2.1. Mechanism

The ACQ effect is opposite to the AIE, as fluorescence is quenched when fluorophores aggregate. ACQ is widely regarded as a disadvantage of fluorophores. Nevertheless, we can harness the ACQ effect to identify nanoparticles and explore their *in vivo* and intracellular fates. A novel series of ACQ probes bearing a BODIPY or an aza-BODIPY parent structure have been developed to explore the *in vivo* fate of drug nanoparticles administered *via* various routes [111–121]. The most distinctive feature of these ACQ probes is water-quenching sensitivity. Contact with water annihilates the fluorescence immediately due to self-aggregation by π-π stacking. Thus, these probes enable real–time tracking of *in vivo* and intracellular translocation. ACQ probes encoded P2 and P4 were embedded for bioimaging of intact cyclosporine A and quercetin nanocrystals, respectively [22,23]. Self-discrimination of hybrid nanocrystals was confirmed by good fluorescent stability, sensitive water-quenching ability, and good correlation between dissolution and fluorescence quenching [22,23].

6.2.2. Transepithelia transportation

Instead of dissolving instantly, nanocrystals may remain intact in the GI tract for an extended time. Live imaging in SD rats orally administered with hybrid nanocrystals showed fluorescent signals for as long as 12–18 h in the GI tract, indicating an unexpectedly long biological life of nanocrystals in the GI tract [22,23]. Then nanocrystals that survive dissolution in the GI tract encounter the enteric epithelia. Surprisingly, hybrid nanocrystals administration can show fluorescence in several organs, such as the liver, lung and spleen, of rats (Fig. 11). These results provide concrete evidence supporting oral absorption of intact nanocrystals throughout the body. The liver is the main terminal organ for absorbed nanocrystals, due to the strong ingestion of macrophages to circulating nanocrystals. Approximately 40% of intravenously injected paclitaxel nanocrystals are captured by the liver within 11 min post-administration [16].

Confocal imaging further supports translocation of nanocrystals *via* the GI membrane. Fluorescent signals were detected on the basolateral side of intestinal membranes of rats treated with both quercetin and cyclosporine A hybrid nanocrystals with ACQ probes (Fig. 12). These results confirm internalization of intact nanocrystals by enteric epithelia. However, absorption of different sized nanocrystals depends on intestinal segments. Jejunum showed higher absorption to smaller nanocrystals than the ileum, which is opposite for bigger nanocrystals. The primary difference between the jejunum and the ileum lies in special structures, such as Peyer's patches (PPs) in the ileum. Follicular-associated epithelial cells (FAE) are enriched in the PPs, where many M cells reside in the FAE region. M cells have been extensively reported to recognize and transport foreign particulates from the lumen to basolateral lymphoid tissues.

6.2.3. Cellular interaction

The Caco-2 cell line is a continuous line of heterogeneous human epithelial colorectal adenocarcinoma cells, which can be differentiated and polarized under specific cultural conditions to resemble the enterocytes lining the small intestine. By co-culturing with HT29-MTX cells, the Caco-2/HT29-MTX model mimics a mucus layer on the surface of cell monolayers. Caco-2 cell models are widely used to predict the absorption of orally administered drugs. Caco-2 cell models also provide a useful *in vitro* tool to validate the transepithelia transportation of nanocrystals *via* oral route.

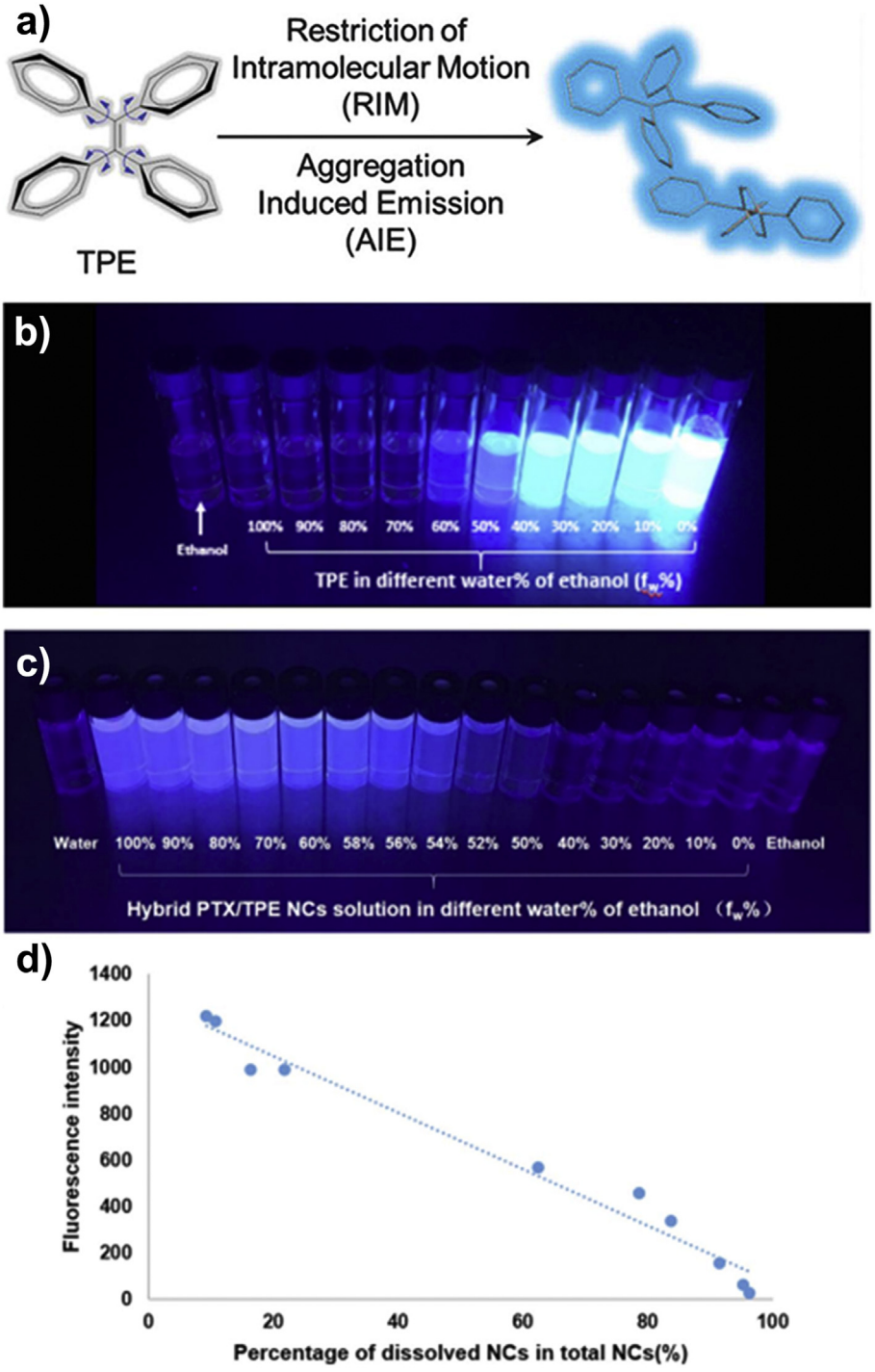

Fig. 9. AIE properties of paclitaxel hybrid nanocrystals with TPE. (a) The propeller-shaped TPE emits fluorescence upon aggregation. (b) TPE and (c) hybrid nanocrystals in water/ethanol mixtures under UV illumination. (d) Fluorescence measurement of hybrid nanocrystals in water/ethanol mixtures at excitation/emission wavelengths of 350 nm/450 nm). Images taken with permission from [21,110].

For both quercetin and cyclosporine A hybrid nanocrystals with ACQ probes, fluorescence was emitted within Caco-2 and Caco-2/HT29-MTX cells, indicating cellular uptake of intact nanocrystals. The fluorescent intensity in Caco-2/HT29-MTX was slightly weaker than that in Caco-2. We concluded that the mucus barrier in the mixed cell model impedes contact of nanocrystals with cell surfaces. Particle size also impacts cellular uptake [122,123]. Cellular uptake of 550 nm quercetin nanocrystals was higher than 280 nm and 1100 nm particles. In contrast, cellular uptake of cyclosporine nanocrystals is linearly opposite to the particle size. The difference between the two nanocrystals relies on different properties of the two drugs, but the exact mechanisms remain unknown. CLSM further confirmed cellular uptake of intact hybrid nanocrystals (Fig. 13). Fluorescent signals occurred in the horizontal plane of the cell nucleus, indicating cellular uptake of intact nanocrystals. Due to the mucous barrier, fluorescence signals in Caco-2 cells were stronger than in the Caco-2/HT29-MTX cells. Moreover, z-axis scanning found fluorescence signals in the basolateral side of both two cell monolayers (Fig. 13, indicated by arrows). These results imply that nanocrystals can not only be taken up by cells, but also be excreted across cell membranes.

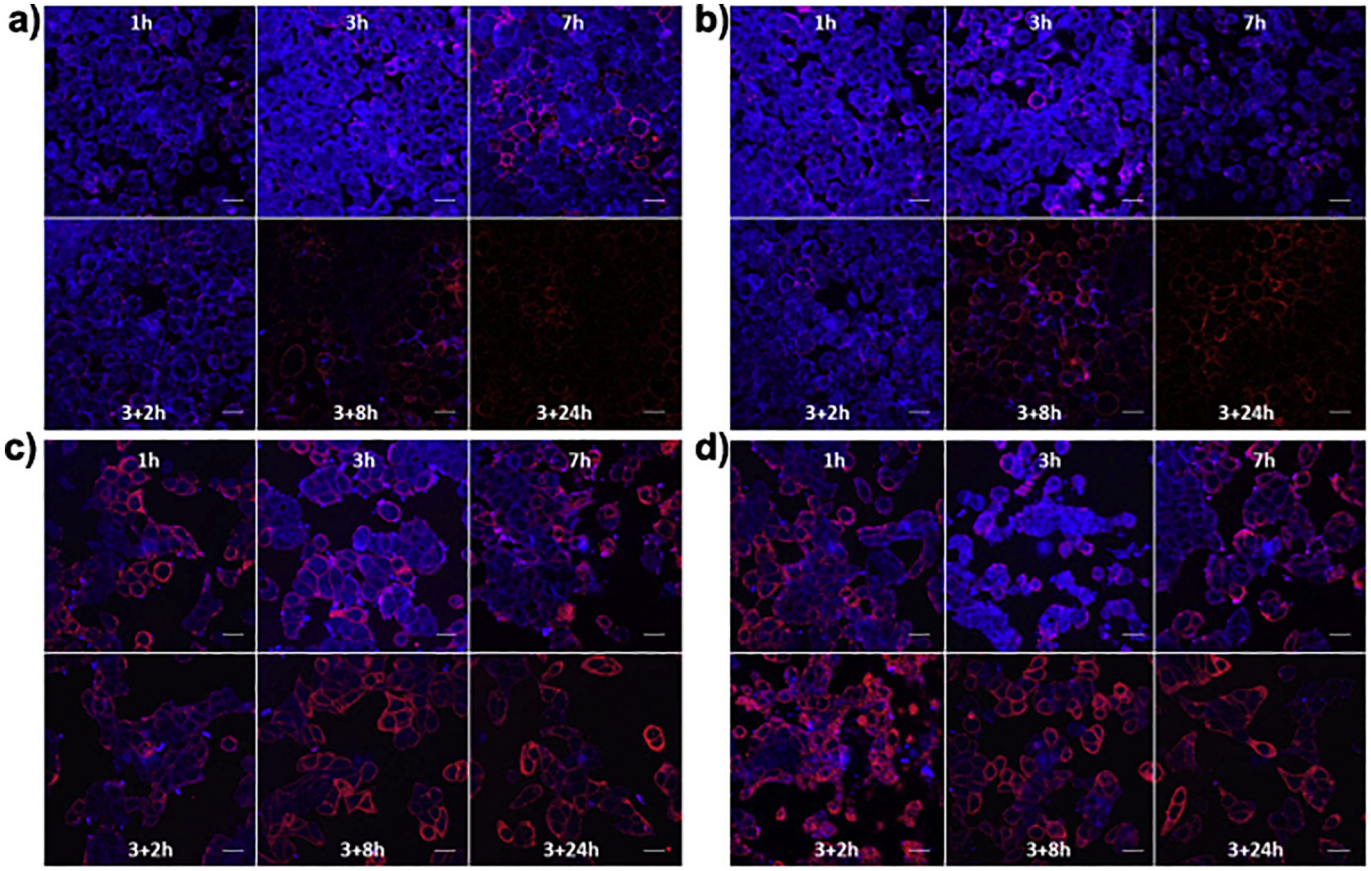

Fig. 10. CLSM images of (a and b) KB and (c and d) HT-29 cells cultured with (a and c) paclitaxel/TPE hybrid nanocrystals and (b and d) F68 modified hybrid nanocrystals using two incubation methods: continuous incubation with nanocrystals for 1, 3, and 7 h or incubation with nanocrystals for 3 h followed by an additional 2, 8, or 24 h incubation with blank medium. Image taken with permission from [21].

6.3. Integration with FRET probes

6.3.1. Concept

FRET describes non-radiative energy transfer from a fluorophore in an excited state (donor) to another chromophore (acceptor) [124]. FRET occurs when the donor and the acceptor are located in close proximity, provided that the emission spectrum of the donor overlaps with the excitation of the acceptor. FRET is extremely sensitive to small changes in distance between the two chromophores, with the fluorescence intensity inversely proportional to the sixth power of the distance. When incorporated into nanocrystals, the donor/acceptor pairs reside closely and can lead to FRET. Once the pairs are released from the nanocrystals, the energy transfer becomes impeded, losing the FRET emission (F_{FRET}) but permitting the donor emission (F_D) [125]. By monitoring F_{FRET}/F_D or relative FRET efficiency, $F_{FRET}/(F_{FRET} + F_D)$, it is possible to assess the structural change of drug nanocrystals. Embedded FRET pairs may allow real-time monitoring of *in vivo* integrity, as well as uptake and intracellular dissolution kinetics of nanocarriers [126–134].

One study described integrating a FRET pair composed of DiO (donor, Ex/Em 484/505 nm) and DiI (acceptor, Ex/Em 549/565 nm) with schisantherin A nanocrystals [104]. Due to the close proximity of DiO and DiI in the nanocrystals, an excitation wavelength (λ_{ex}^{DiO}) of 420 nm could differentiate DiO and DiI (Fig. 14 a). When suspended in water, the hybrid nanocrystals exhibited a strong emission (λ_{em}^{DiI}) peak at 565 nm with a FRET efficiency of 0.95 ± 0.01 (Fig. 14b). In contrast, dissolution in acetone exhibited a significant increase in emission at 505 nm (F_D) with a 0.25 decrease in FRET efficiency, possibly due to dissociation of the FERT pair. Thus, the FRET efficiency corresponds to the integrity of hybrid nanocrystals. Variability in the FRET ratio can monitor the real-time intracellular release of nanocrystals, as discussed below.

6.3.2. Intracellular dissolution and trans-monolayer transportation

Integrity of schisantherin A hybrid nanocrystals inside MDCK cells was monitored by embedding FRET pair (DiO/DiI) in the crystals [104]. After incubation with MDCK cells, schisantherin A hybrid nanocrystals internalized based on strong cellular FRET signals. One hour after incubation, the extracellular medium was replaced by fresh PBS. The FRET ratio decreased from 0.92 to 0.63 over the next 60 min, suggesting dissolution of nanocrystals inside the cells and release of the FRET pairs (Fig. 15). Then, transmonolayer of the nanocrystals was performed on Transwell. MDCK cells are derived from Madin-Darby canine kidney, possessing a mucus layer, polarity and tight junctions similar to the intestinal epithelium. At 2 h, the FRET ratio in the apical chamber decreased slightly from 0.95 to 0.90, suggesting that most nanocrystals remained undissolved during incubation. The FRET ratio in the basolateral chamber was only 0.36. These results suggested transportation of nanocrystals across the cell monolayer, although some ingested nanocrystals did dissolve inside the cells.

6.4. Limitations of environmental-sensitive probes

Organic AIE nanoparticles are well-established for cell tracking [135], vascular imaging [136], tumor imaging and therapy [137]. Encapsulating more AIE fluorophores can enhance nanoparticle brightness [138]. However, encapsulating more conventional fluorophores inside nanocarriers may quench photoluminescence, resulting in low brightness or even completely quenching fluorescence [139]. To exclusively mark nanocrystals, released AIE molecules from dissolved nanocrystals

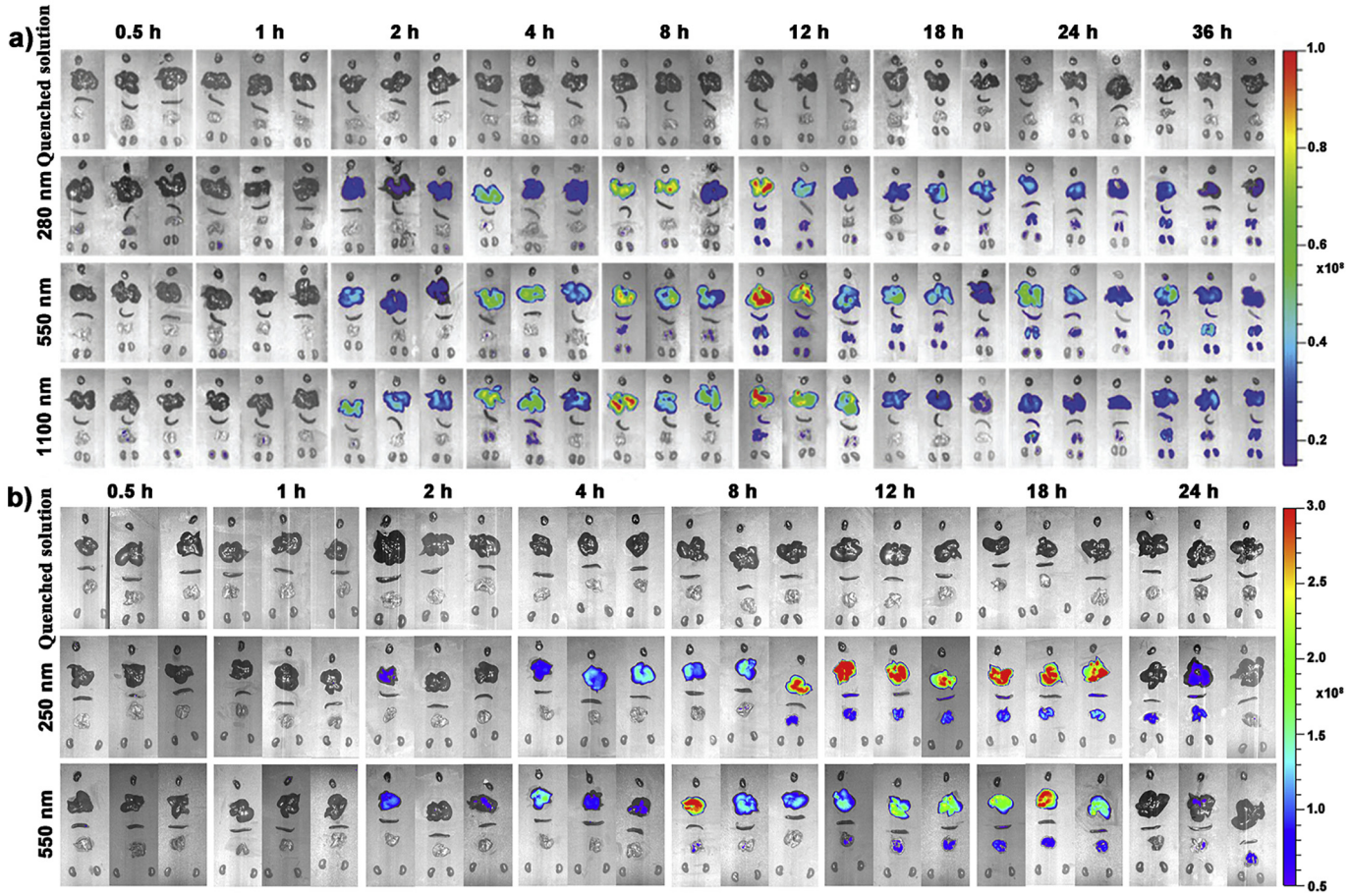

Fig. 11. *In vivo* live imaging for SD rats after gavage administration of (a) quercetin and (b) cyclosporine A hybrid nanocrystals of different sizes. Images taken with permission from [22,23].

must remain soluble or dispersed, as fluorophore aggregation can also generate AIE [140–142]. Using this rationale, we assumed two extremes in which the released AIE probes either completely recrystallized or entirely dissolved when calculating nanocrystal disintegration [21]. In addition, the emission wavelength of AIE probes is generally shorter than 600 nm, which limits their application *in vivo* due to autofluorescence. Recent developments in near-infrared AIE probes [143–145] will expand the application of AIE based hybrid nanocrystals from cellular studies to whole-body tracking.

However, self-association of ACQ probes can quench fluorescence. So, interference from precipitates of released probes, which is associated with using AIE probes, should be avoided. The fluorescence intensity of hybrid nanocrystals with ACQ like AIE probes quantitatively corresponds to nanocrystal amount [22,23]. Yet, "re-kindling" of ACQ probes due to disaggregation poses a serious concern. Dramatic changes in the cellular environment can lead to dissociation of ACQ aggregates to monomers, which can recover the fluorescence. Faint fluorescence was observed in animals treated by the quenched solution of ACQ probes, likely due to solubilizing ACQ aggregates by lipid or other lipophilic molecules in the biological milieu [22,23]. Therefore, evaluating the level of "re-kindling" must include a quenched ACQ solution with the equivalent ACQ concentration to the delivery system as a background.

Compared with AIE and ACQ probes, using FRET donor/acceptor pairs for tracing nanocrystals poses additional complications in measurements and analysis. FRET provides not only a qualitative but also a semi-quantitative assessment of hybrid nanoparticle integrity. The generation of the standard curve for analysis requires measurements of F_{FRET} and F_D from mixtures of FRET loaded nanoparticles, as well as nanoparticles encapsulating the donor and acceptor [146]. Selection of donor and acceptor fluorophores affects FRET applications and minimizes ambiguity in imaging results. Commonly used FRET pairs are summarized in Table 2. A large overlap (J) between the donor and acceptor spectrum is the most important consideration to maximize FRET stability and cross talk between the donor and acceptor [147]. Highly efficient FRET pairs still bear non-negligible spectral bleed-through (SBT) in their excitation (Ex SBT) or emission (Em SBT) spectra [125], which indicates the fluorescence intensities of the two chromophores must be comparable. If this guideline is not followed, the stronger one will shadow the measurement of the weaker one, leading to unreliable FRET efficiency [148]. Another source of ambiguity in FRET imaging is poor fluorescence stability, which includes environmental stability and photostability.

7. Conclusions and outlook

Nanocrystal formulation enables delivery of poorly soluble drugs and offers key advantages over conventional techniques [9]. In addition to oral and intravenous delivery, nanocrystal formulations have shown great potentials in drug delivery *via* transdermal, ocular, and pulmonary routes [10,44–47,149]. With the ongoing discovery of more poorly soluble drugs, the need for nanocrystal-base products will become critical in developing novel strategies to determine and understand the *in vivo* fate of these products.

The hybrid nanocrystal concept provides a platform tool for bioimaging of nanocrystals *in vivo*. Embedding fluorescent probes in drug nanocrystals does not require extra steps in the preparation of nanocrystals, which adds another advantage for utilizing hybrid nanocrystals as a unique theranostic tool. Integrated dye molecules produce little effect on the crystallinity and other particle properties of drug nanocrystals. The mass content of fluorescent probe molecules in the

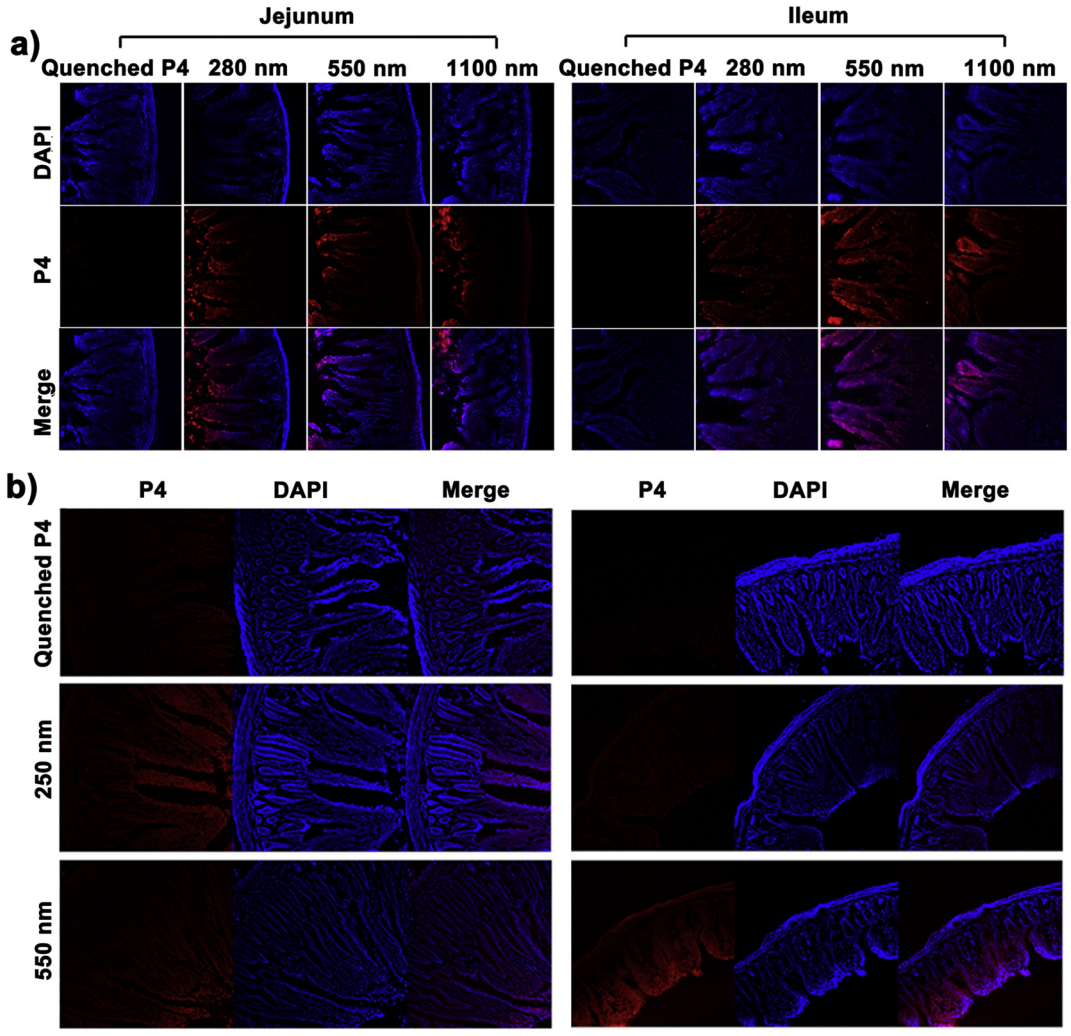

Fig. 12. CLSM photos of frozen sections from the jejunum and ileum of rats treated by different sizes of (a) quercetin and (b) cyclosporine A hybrid nanocrystals. Images adopted with permission from [22,23].

host nanocrystals is trivial. Hybrid nanocrystals can be measured by IVIS or CLSM. Moreover, environment-responsive fluorophores show greater utility than conventional probes due to the dissolution of the crystals. AIE, ACQ, and FRET probes may illuminate drug hybrid nanocrystals, though further development may be required for broader testing. The FRET pairs are restrained to semi-quantitative, while NIR AIE probes are required for *in vivo* study. Nonetheless, possible "re-kindling" of released probes due to precipitation (*e.g.*, AIE) or dispersion in hydrophobic biologic media (*e.g.*, ACQ) are considerations when analyzing bioimaging data.

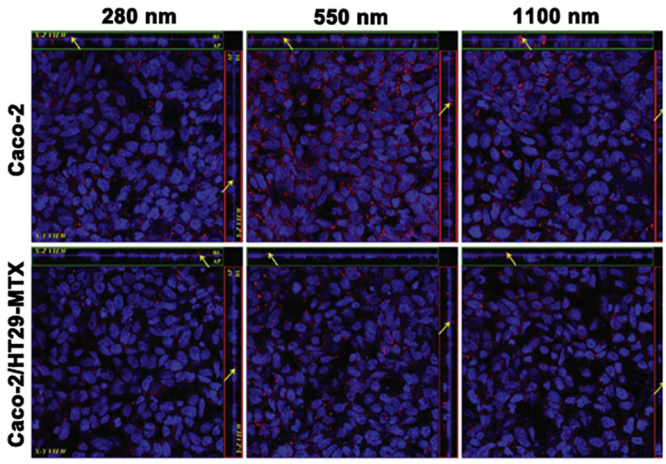

Fig. 13. CLSM images of Caco-2 and Caco-2/HT29-MTX monolayers treated with quercetin hybrid nanocrystals of different sizes. Image taken with permission from [23].

Kinetic information of the *in vivo* and intracellular fate of several nanocrystals continue to add to our knowledge [19,21–23]. This developing area is key since nanocrystals can be retained in the body for extended periods of time instead of dissolving instantly. Undissolved nanocrystals are exposed to cells and tissues. Drug nanocrystals circulating in the blood stream can reach tumor sites by as much as a few percent, while some nanocrystals in the GI tract are transported across the intestinal epithelia and accumulate in main organs. Cellular studies confirm the uptake of whole nanocrystals, which dissolve inside the cell and/or are excreted by exocytosis. Our observations indicate that one nanocrystal data may not be extrapolated to other nanocrystal systems, as individual variation among nanocrystals are extensive due to diversity in physicochemical properties of the drugs. Quantitative evaluation of spatial and temporal transportation and distribution of nanocrystals and dissolved molecules continues to remain a significant challenge in drug development for clinical use. It is thus vital to consider the contribution of nanocrystals to the overall bioavailability and distribution of delivered drugs. Moreover, while the information is limited in the literature, it is expected that particle properties of drug nanocrystals

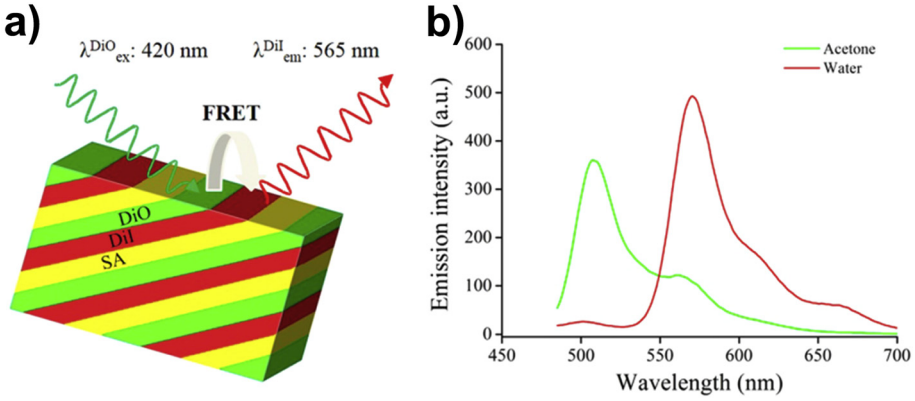

Fig. 14. FRET analysis of hybrid Schisantherin A nanocrystals with DiO and DiI. (a) A schematic diagram for FRET signal from the hybrid nanocrystals. (b) Fluorescence spectra of the hybrid nanocrystals in water and acetone. Image taken with permission from [104].

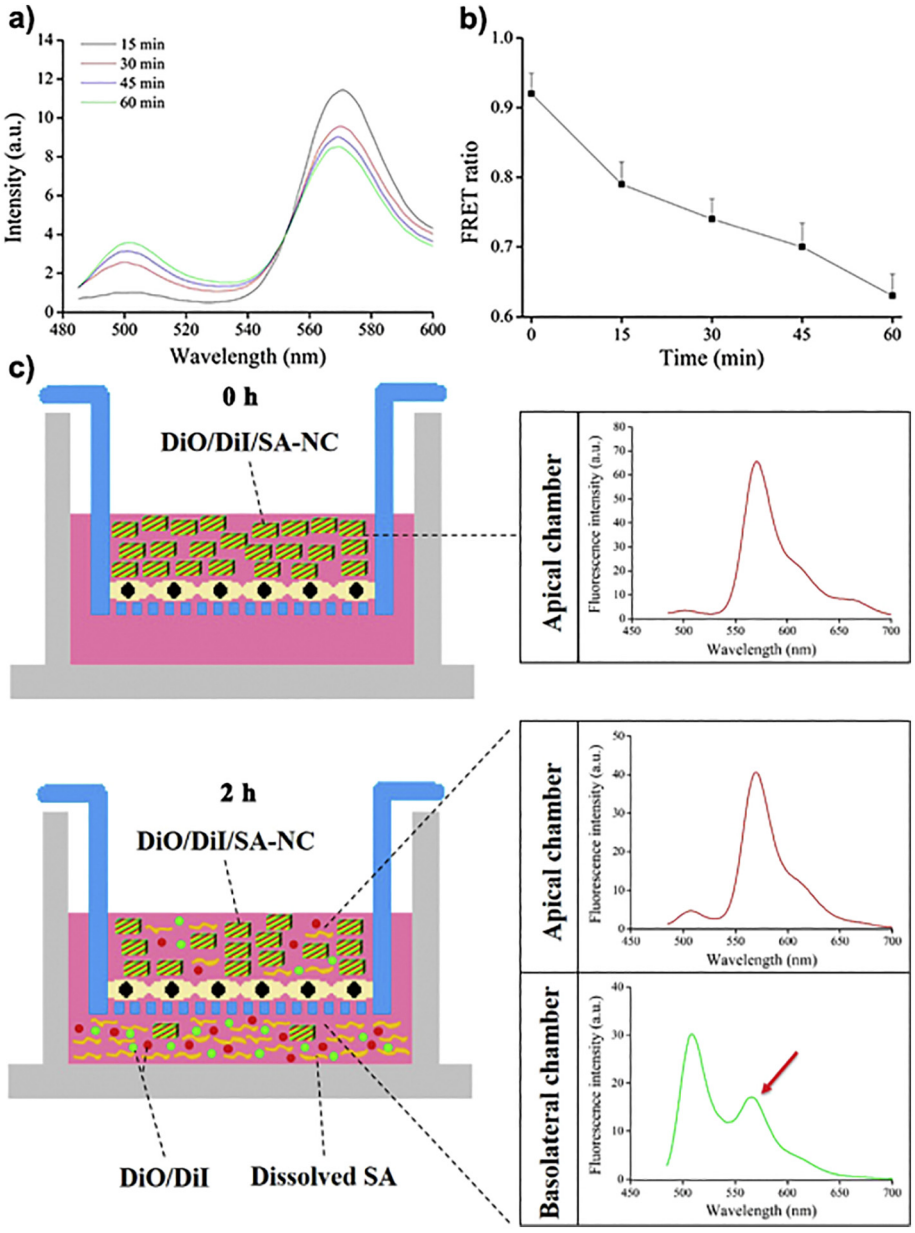

Fig. 15. Dissolution of schisantherin A hybrid nanocrystals inside MDCK cells indicated by the change in (a) fluorescence intensity and (b) FRET ratio of the cells after incubation in fresh pH 7.4 PBS. (c) Fluorescence spectrum before and 2 h after transport studies (red arrow indicates FRET). Image taken with permission from [104].

Table 2
Commonly Used Donor-Acceptor FRET Pairs. The Table is Adopted With Permission from [125].

Donor	Acceptor	J[a] (M^{-1} cm^{-1} nm^4)	R_0[b] (nm)	BR ratio[c]	Ex SBT[d] (%)	Em SBT[e] (%)
Cy3	Cy5	4.68×10^{15}	5.49	1.6:1	6	4
Cy3	Cy5.5	4.64×10^{15}	5.48	1.1:1	3	2
Cy3.5	Cy5	9.21×10^{15}	6.27	1.4:1	11	15
Cy3.5	Cy5.5	1.10×10^{16}	6.45	1:1	6	8
Cy5	Cy7	1.52×10^{16}	6.21	1:2	12	3
Cy5	Cy7.5	6.60×10^{15}	5.40	1:2.2	4	1
Cy5.5	Cy7	2.57×10^{16}	6.78	1:1.4	17	10
Cy5.5	Cy7.5	1.63×10^{15}	6.28	1:1.6	7	8
DiO	DiI	5.60×10^{15}	4.02	1:1.7	11	12
DiD	DiR	2.42×10^{16}	7.29	1.2:1	12	5

[a] Spectral overlap integral.
[b] Förster distance, *i.e.* the distance at which the energy transfer efficiency is 50%.
[c] Brightness ratio.
[d] Spectral bleed-through between donor and acceptor excitation.
[e] Spectral bleed-through between donor and acceptor emission.

including size, shape, and surface chemistry should have profound effects on the *in vivo* fate, pharmacokinetics, and cellular interaction. The hybrid nanocrystal approach will thus enable findings of the impact of the particle properties.

We argue that hybrid nanocrystals remain a promising avenue to develop novel and more efficacious therapeutic strategies. Expanding the hybrid nanocrystal technique to the drug delivery *via* transdermal, ocular, and pulmonary routes will further development of nanocrystal-based formulation targeting these routes. Hybrid nanocrystals embedding inorganic or metal contrast agents, radioisotopes, or superparamagnetic probes will enable other types of bioimaging modalities, in addition to fluorescent imaging, potentially providing comprehensive characterization of *in vivo* and intracellular kinetics of nanocrystals. The understanding hold tremendous significance to enable nanocrystal formulation and development. Integration of other types of synergistic molecules than bioimaging agents in drug nanocrystals, such as targeting compounds, could further expand the application of nanocrystal-based drug delivery systems.

Acknowledgements

This work was supported by the National Natural Science Foundation of China [81872815, 81573363, 81690263]; and the Natural Science Foundation of Shanghai [16ZR1403500]. TL is thankful to Chao Endowment. We thank Life Science Editors for editing assistance.

References

[1] H.D. Williams, N.L. Trevaskis, S.A. Charman, R.M. Shanker, W.N. Charman, C.W. Pouton, C.J. Porter, Strategies to address low drug solubility in discovery and development, Pharmacol. Rev. 65 (1) (2013) 315–499.
[2] P. Shekhawat, V. Pokharkar, Understanding peroral absorption: regulatory aspects and contemporary approaches to tackling solubility and permeability hurdles, Acta Pharm. Sin. B 7 (3) (2017) 260–280.
[3] V. Sharma, K. Pathak, Effect of hydrogen bond formation/replacement on solubility characteristics, gastric permeation and pharmacokinetics of curcumin by application of powder solution technology, Acta Pharm. Sin. B 6 (6) (2016) 600–613.
[4] J. Leleux, R.O. Williams, Recent advancements in mechanical reduction methods: particulate systems, Drug Dev. Ind. Pharm. 40 (3) (2014) 289–300.
[5] Z.H. Loh, A.K. Samanta, P.W.S. Heng, Overview of milling techniques for improving the solubility of poorly water-soluble drugs, Asian J. Pharm. Sci. 10 (4) (2015) 255–274.
[6] N. Rasenack, B.W. Muller, Micron-size drug particles: common and novel micronization techniques, Pharm. Dev. Technol. 9 (1) (2004) 1–13.
[7] E.M. Merisko-Liversidge, G.G. Liversidge, Drug nanoparticles: formulating poorly water-soluble compounds, Toxicol. Pathol. 36 (1) (2008) 43–48.
[8] L. Gao, D. Zhang, M. Chen, Drug nanocrystals for the formulation of poorly soluble drugs and its application as a potential drug delivery system, J. Nanopart. Res. 10 (5) (2008) 845–862.
[9] R. Shegokar, R.H. Muller, Nanocrystals: industrially feasible multifunctional formulation technology for poorly soluble actives, Int. J. Pharm. 399 (1–2) (2010) 129–139.
[10] R.H. Muller, S. Gohla, C.M. Keck, State of the art of nanocrystals - special features, production, nanotoxicology aspects and intracellular delivery, Eur. J. Pharm. Biopharm. 78 (1) (2011) 1–9.
[11] E. Merisko-Liversidge, G.G. Liversidge, Nanosizing for oral and parenteral drug delivery: a perspective on formulating poorly-water soluble compounds using wet media milling technology, Adv. Drug Deliver. Rev. 63 (6) (2011) 427–440.
[12] Y. Lu, Y. Li, W. Wu, Injected nanocrystals for targeted drug delivery, Acta Pharm. Sin. B 6 (2) (2016) 106–113.
[13] Y. Lu, Y. Chen, R.A. Gemeinhart, W. Wu, T. Li, Developing nanocrystals for cancer treatment, Nanomedicine (Lond) 10 (16) (2015) 2537–2552.
[14] Y. Lu, J. Qi, X. Dong, W. Zhao, W. Wu, The in vivo fate of nanocrystals, Drug Discov. Today 22 (4) (2017) 744–750.
[15] T. Li, Hybrid Nanocrystals for Treatment and Bioimaging of Disease, 2006 US20060280680Al.
[16] C.P. Hollis, H.L. Weiss, M. Leggas, B.M. Evers, R.A. Gemeinhart, T. Li, Biodistribution and bioimaging studies of hybrid paclitaxel nanocrystals: lessons learned of the EPR effect and image-guided drug delivery, J. Control. Release 172 (1) (2013) 12–21.
[17] C.P. Hollis, H.L. Weiss, B.M. Evers, R.A. Gemeinhart, T. Li, In vivo investigation of hybrid paclitaxel nanocrystals with dual fluorescent probes for cancer theranostics, Pharm. Res. 31 (6) (2014) 1450–1459.
[18] R. Zhao, C.P. Hollis, H. Zhang, L. Sun, R.A. Gemeinhart, T. Li, Hybrid nanocrystals: achieving concurrent therapeutic and bioimaging functionalities toward solid tumors, Mol. Pharm. 8 (5) (2011) 1985–1991.
[19] Y. Chen, T. Li, Cellular uptake mechanism of paclitaxel nanocrystals determined by confocal imaging and kinetic measurement, AAPS J. 17 (5) (2015) 1126–1134.
[20] C.P. Hollis, A.K. Dozier, B.L. Knutson, T. Li, Preparation and characterization of multimodal hybrid organic and inorganic nanocrystals of camptothecin and gold, Acta Pharm. Sin. B 9 (1) (2019) 128–134.
[21] W. Gao, D. Lee, Z. Meng, T. Li, Exploring intracellular fate of drug nanocrystals with crystal-integrated and environment-sensitive fluorophores, J. Control. Release 267 (2017) 214–222.
[22] Y. Xie, B. Shi, F. Xia, J. Qi, X. Dong, W. Zhao, T. Li, W. Wu, Y. Lu, Epithelia transmembrane transport of orally administered ultrafine drug particles evidenced by environment sensitive fluorophores in cellular and animal studies, J. Control. Release 270 (2018) 65–75.
[23] C. Shen, Y. Yang, B. Shen, Y. Xie, J. Qi, X. Dong, W. Zhao, W. Zhu, W. Wu, H. Yuan, Y. Lu, Self-discriminating fluorescent hybrid nanocrystals: efficient and accurate tracking of translocation via oral delivery, Nanoscale 10 (1) (2017) 436–450.
[24] R.H. Muller, C. Jacobs, O. Kayser, Nanosuspensions as particulate drug formulations in therapy: rationale for development and what we can expect for the future, Adv. Drug Deliver. Rev. 47 (1) (2001) 3–19.
[25] B.E. Rabinow, Nanosuspensions in drug delivery, Nat. Rev. Drug Discov. 3 (9) (2004) 785–796.
[26] J.J. Ma, Y.X. Yang, Y.H. Sun, J. Sun, Optimization, characterization and in vitro/vivo evaluation of azilsartan nanocrystals, Asian J. Pharm. Sci. 12 (4) (2017) 344–352.
[27] F. Toziopoulou, M. Malamatari, I. Nikolakakis, K. Kachrimanis, Production of aprepitant nanocrystals by wet media milling and subsequent solidification, Int. J. Pharm. 533 (2) (2017) 324–334.
[28] L. Ye, M. Miao, S. Li, K. Hao, Nanosuspensions of a new compound, ER-beta 005, for enhanced oral bioavailability and improved analgesic efficacy, Int. J. Pharm. 531 (1) (2017) 246–256.
[29] L. Zong, X. Li, H. Wang, Y. Cao, L. Yin, M. Li, Z. Wei, D. Chen, X. Pu, J. Han, Formulation and characterization of biocompatible and stable IV itraconazole nanosuspensions stabilized by a new stabilizer polyethylene glycol-poly (beta-benzyl-L-aspartate) (PEG-PBLA), Int. J. Pharm. 531 (1) (2017) 108–117.
[30] M.M. Chogale, V.N. Ghodake, V.B. Patravale, Performance parameters and characterizations of nanocrystals: a brief review, Pharmaceutics 8 (3) (2016) 26.
[31] A. Tuomela, J. Hirvonen, L. Peltonen, Stabilizing agents for drug nanocrystals: effect on bioavailability, Pharmaceutics 8 (2) (2016) 16.
[32] Y. Barenholz, Doxil(R)–the first FDA-approved nano-drug: lessons learned, J. Control. Release 160 (2) (2012) 117–134.
[33] C.F. Huang, K.S. Liang, T.L. Hsu, T.T. Lee, Y.Y. Chen, S.M. Yang, H.H. Chen, S.H. Huang, W.H. Chang, T.K. Lee, P. Chen, K.E. Peng, C.C. Chen, C.Z. Shi, Y.F. Hu, G. Margaritondo, T. Ishikawa, C.H. Wong, Y. Hwu, Free-electron-laser coherent diffraction images of individual drug-carrying liposome particles in solution, Nanoscale 10 (6) (2018) 2820–2824.
[34] E. Merisko-Liversidge, G.G. Liversidge, E.R. Cooper, Nanosizing: a formulation approach for poorly-water-soluble compounds, Eur. J. Pharm. Sci. 18 (2) (2003) 113–120.
[35] R. Shegokar, K.K. Singh, Surface modified nevirapine nanosuspensions for viral reservoir targeting: in vitro and in vivo evaluation, Int. J. Pharm. 421 (2) (2011) 341–352.
[36] K. Fuhrmann, M.A. Gauthier, J.C. Leroux, Targeting of injectable drug nanocrystals, Mol. Pharm. 11 (6) (2014) 1762–1771.
[37] S.E. Lee, S.F. Bairstow, J.O. Werling, M.V. Chaubal, L. Lin, M.A. Murphy, J.P. DiOrio, J. Gass, B. Rabinow, X. Wang, Y. Zhang, Z. Yang, R.M. Hoffman, Paclitaxel nanosuspensions for targeted chemotherapy - nanosuspension preparation, characterization, and use, Pharm. Dev. Technol. 19 (4) (2014) 438–453.
[38] M. Talekar, S. Ganta, M. Amiji, S. Jamieson, J. Kendall, W.A. Denny, S. Garg, Development of PIK-75 nanosuspension formulation with enhanced delivery efficiency and cytotoxicity for targeted anti-cancer therapy, Int. J. Pharm. 450 (1–2) (2013) 278–289.

[39] N. Hernandez, Ryanodex®-So Easy to Use, Even a Caveman can do it! http://blog.clinicalmonster.com/2017/11/ryanodex-easy-use-even-caveman-can/ 2017 (updated 27/12/2018).
[40] G.G. Liversidge, K.C. Cundy, J.F. Bishop, D.A. Czekai, Surface Modified Drug Nanoparticles, 1992 US005145684A.
[41] G.G. Liversidge, K.C. Cundy, Particle-size reduction for improvement of oral bioavailability of hydrophobic drugs. 1. absolute oral bioavailability of nanocrystalline danazol in beagle dogs, Int. J. Pharm. 125 (1) (1995) 91–97.
[42] G.G. Liversidge, P. Conzentino, Drug particle-size reduction for decreasing gastric irritancy and enhancing absorption of naproxen in rats, Int. J. Pharm. 125 (2) (1995) 309–313.
[43] A. Hanafy, H. Spahn-Langguth, G. Vergnault, P. Grenier, M. Tubic Grozdanis, T. Lenhardt, P. Langguth, Pharmacokinetic evaluation of oral fenofibrate nanosuspensions and SLN in comparison to conventional suspensions of micronized drug, Adv. Drug Deliver. Rev. 59 (6) (2007) 419–426.
[44] G.B. Romero, A. Arntjen, C.M. Keck, R.H. Muller, Amorphous cyclosporin a nanoparticles for enhanced dermal bioavailability, Int. J. Pharm. 498 (1–2) (2016) 217–224.
[45] O.P. Sharma, V. Patel, T. Mehta, Nanocrystal for ocular drug delivery: hope or hype, Drug Deliv. Transl. Res. 6 (4) (2016) 399–413.
[46] V.K. Pawar, Y. Singh, J.G. Meher, S. Gupta, M.K. Chourasia, Engineered nanocrystal technology: in-vivo fate, targeting and applications in drug delivery, J. Control. Release 183 (2014) 51–66.
[47] L. Gao, G. Liu, J. Ma, X. Wang, L. Zhou, X. Li, Drug nanocrystals: in vivo performances, J. Control. Release 160 (3) (2012) 418–430.
[48] R.C. Nagarwal, R. Kumar, M. Dhanawat, N. Das, J.K. Pandit, Nanocrystal technology in the delivery of poorly soluble drugs: an overview, Curr. Drug Deliv. 8 (4) (2011) 398–406.
[49] B. Sinha, R.H. Muller, J.P. Moschwitzer, Bottom-up approaches for preparing drug nanocrystals: formulations and factors affecting particle size, Int. J. Pharm. 453 (1) (2013) 126–141.
[50] H. de Waard, H.W. Frijlink, W.L. Hinrichs, Bottom-up preparation techniques for nanocrystals of lipophilic drugs, Pharm. Res. 28 (5) (2011) 1220–1223.
[51] V.B. Patravale, A.A. Date, R.M. Kulkarni, Nanosuspensions: a promising drug delivery strategy, J. Pharm. Pharmacol. 56 (7) (2004) 827–840.
[52] X. Ren, J. Qi, W. Wu, Z. Yin, T. Li, Y. Lu, Development of carrier-free nanocrystals of poorly water-soluble drugs by exploring metastable zone of nucleation, Acta Pharm. Sin. B (2018) https://doi.org/10.1016/j.apsb.2018.1005.1004.
[53] D. Xia, Y. Gan, F. Cui, Application of precipitation methods for the production of water-insoluble drug nanocrystals: production techniques and stability of nanocrystals, Curr. Pharm. Des. 20 (3) (2014) 408–435.
[54] R.S. Dhumal, S.V. Biradar, S. Yamamura, A.R. Paradkar, P. York, Preparation of amorphous cefuroxime axetil nanoparticles by sonoprecipitation for enhancement of bioavailability, Eur. J. Pharm. Biopharm. 70 (1) (2008) 109–115.
[55] V. Kumar, L. Wang, M. Riebe, H.H. Tung, R.K. Prud'homme, Formulation and stability of itraconazole and odanacatib nanoparticles: governing physical parameters, Mol. Pharm. 6 (4) (2009) 1118–1124.
[56] M. Guo, Q. Fu, C. Wu, Z. Guo, M. Li, J. Sun, Z. He, L. Yang, Rod shaped nanocrystals exhibit superior in vitro dissolution and in vivo bioavailability over spherical like nanocrystals: a case study of lovastatin, Colloid. Surface. B 128 (2015) 410–418.
[57] T. Thao Truong-Dinh, T. Kiet Anh, T. Phuong Ha-Lien, Modulation of particle size and molecular interactions by sonoprecipitation method for enhancing dissolution rate of poorly water-soluble drug, Ultrason. Sonochem. 24 (2015) 256–263.
[58] T. Jiang, N. Han, B. Zhao, Y. Xie, S. Wang, Enhanced dissolution rate and oral bioavailability of simvastatin nanocrystal prepared by sonoprecipitation, Drug Dev. Ind. Pharm. 38 (10) (2012) 1230–1239.
[59] T. Thao Truong-Dinh, T. Phuong Ha-Lien, N. Minh Ngoc, T. Khanh Thi My Uyen, P. Minh Nguyet, T. Phuc Cao, V. Toi Van, Amorphous isradipine nanosuspension by the sonoprecipitation method, Int. J. Pharm. 474 (1–2) (2014) 146–150.
[60] S.M. D'Addio, R.K. Prud'homme, Controlling drug nanoparticle formation by rapid precipitation, Adv. Drug Deliver. Rev. 63 (6) (2011) 417–426.
[61] Y. Dong, W.K. Ng, S. Shen, S. Kim, R.B.H. Tan, Controlled antisolvent precipitation of spironolactone nanoparticles by impingement mixing, Int. J. Pharm. 410 (1–2) (2011) 175–179.
[62] C. Beck, S.V. Dalvi, R.N. Dave, Controlled liquid antisolvent precipitation using a rapid mixing device, Chem. Eng. Sci. 65 (21) (2010) 5669–5675.
[63] S.W. Siddiqui, P.J. Unwin, Z. Xu, S.M. Kresta, The effect of stabilizer addition and sonication on nanoparticle agglomeration in a confined impinging jet reactor, Colloid Surface. A 350 (1–3) (2009) 38–50.
[64] H. Chiou, H.K. Chan, R.K. Prud'homme, J.A. Raper, Evaluation on the use of confined liquid impinging jets for the synthesis of nanodrug particles, Drug Dev. Ind. Pharm. 34 (1) (2008) 59–64.
[65] Y. Liu, C. Cheng, Y. Liu, R.K. Prud'homme, R.O. Fox, Mixing in a multi-inlet vortex mixer (MIVM) for flash nano-precipitation, Chem. Eng. Sci. 63 (11) (2008) 2829–2842.
[66] J.F. Chen, M.Y. Zhou, L. Shao, Y.Y. Wang, J. Yun, N.Y. Chew, H.K. Chan, Feasibility of preparing nanodrugs by high-gravity reactive precipitation, Int. J. Pharm. 269 (1) (2004) 267–274.
[67] T. Hu, J. Wang, Z. Shen, J. Chen, Engineering of drug nanoparticles by HGCP for pharmaceutical applications, Particuology 6 (4) (2008) 239–251.
[68] J.F. Chen, Y.H. Wang, F. Guo, X.M. Wang, C. Zheng, Synthesis of nanoparticles with novel technology: high-gravity reactive precipitation, Ind. Eng. Chem. Res. 39 (4) (2000) 948–954.
[69] S.G. Kwon, T. Hyeon, Formation mechanisms of uniform nanocrystals via hot-injection and heat-up methods, Small 7 (19) (2011) 2685–2702.
[70] T. Sugimoto, Underlying mechanisms in size control of uniform nanoparticles, J. Colloid Interf. Sci 309 (1) (2007) 106–118.
[71] B. Rabinow, J. Kipp, P. Papadopoulos, J. Wong, J. Glosson, J. Gass, C.-S. Sun, T. Wielgos, R. White, C. Cook, K. Barker, K. Wood, Itraconazole IV nanosuspension enhances efficacy through altered pharmacokinetics in the rat, Int. J. Pharm. 339 (1–2) (2007) 251–260.
[72] Q. Fu, J. Sun, X. Ai, P. Zhang, M. Li, Y. Wang, X. Liu, Y. Sun, X. Sui, L. Sun, X. Han, M. Zhu, Y. Zhang, S. Wang, Z. He, Nimodipine nanocrystals for oral bioavailability improvement: role of mesenteric lymph transport in the oral absorption, Int. J. Pharm. 448 (1) (2013) 290–297.
[73] M. Reifarth, S. Hoeppener, U.S. Schubert, Uptake and intracellular fate of engineered nanoparticles in mammalian cells: capabilities and limitations of transmission electron microscopy-polymer-based nanoparticles, Adv. Mater. 30 (9) (2018) 1703704.
[74] Z. Guo, S. Park, J. Yoon, I. Shin, Recent progress in the development of near-infrared fluorescent probes for bioimaging applications, Chem. Soc. Rev. 43 (1) (2014) 16–29.
[75] X. He, Y. Ma, M. Li, P. Zhang, Y. Li, Z. Zhang, Quantifying and imaging engineered nanomaterials in vivo: challenges and techniques, Small 9 (9–10) (2013) 1482–1491.
[76] A. Kermanizadeh, D. Balharry, H. Wallin, S. Loft, P. Moller, Nanomaterial translocation–the biokinetics, tissue accumulation, toxicity and fate of materials in secondary organs–a review, Crit. Rev. Toxicol. 45 (10) (2015) 837–872.
[77] J. Yin, Y. Hu, J. Yoon, Fluorescent probes and bioimaging: alkali metals, alkaline earth metals and pH, Chem. Soc. Rev. 44 (14) (2015) 4619–4644.
[78] L. Vidlarova, G.B. Romero, J. Hanus, F. Stepanek, R.H. Muller, Nanocrystals for dermal penetration enhancement - effect of concentration and underlying mechanisms using curcumin as model, Eur. J. Pharm. Biopharm. 104 (2016) 216–225.
[79] X. Miao, Y. Li, X. Wang, S.M.-Y. Lee, Y. Zheng, Transport mechanism of coumarin 6 nanocrystals with two particle sizes in MDCKII monolayer and larval zebrafish, ACS Appl. Mater. Interfaces 8 (20) (2016) 12620–12630.
[80] C.P. Chan, Y. Bruemmel, M. Seydack, K.K. Sin, L.W. Wong, E. Merisko-Liversidge, D. Trau, R. Renneberg, Nanocrystal biolabels with releasable fluorophores for immunoassays, Anal. Chem. 76 (13) (2004) 3638–3645.
[81] A.A. Noyes, W.R. Whitney, The rate of solution of solid substances in their own solutions, J. Am. Chem. Soc. 19 (12) (1897) 930–934.
[82] L. Gao, D. Zhang, M. Chen, C. Duan, W. Dai, L. Jia, W. Zhao, Studies on pharmacokinetics and tissue distribution of oridonin nanosuspensions, Int. J. Pharm. 355 (1–2) (2008) 321–327.
[83] K. Sigfridsson, S. Forssen, P. Hollander, U. Skantze, J. de Verdier, A formulation comparison, using a solution and different nanosuspensions of a poorly soluble compound, Eur. J. Pharm. Biopharm. 67 (2) (2007) 540–547.
[84] L. Hao, J. Luan, D. Zhang, C. Li, H. Guo, L. Qi, X. Liu, T. Li, Q. Zhang, Research on the in vitro anticancer activity and in vivo tissue distribution of Amoitone B nanocrystals, Colloid. Surface. B 117 (2014) 258–266.
[85] R. Shegokar, K.K. Singh, Nevirapine nanosuspensions for HIV reservoir targeting, Pharmazie. 66 (6) (2011) 408–415.
[86] L. Hao, X. Wang, D. Zhang, Q. Xu, S. Song, F. Wang, C. Li, H. Guo, Y. Liu, D. Zheng, Q. Zhang, Studies on the preparation, characterization and pharmacokinetics of Amoitone B nanocrystals, Int. J. Pharm. 433 (1–2) (2012) 157–164.
[87] M. Han, X. Liu, Y. Guo, Y. Wang, X. Wang, Preparation, characterization, biodistribution and antitumor efficacy of hydroxycamptothecin nanosuspensions, Int. J. Pharm. 455 (1–2) (2013) 85–92.
[88] H. Zhang, X. Wang, W. Dai, R.A. Gemeinhart, Q. Zhang, T. Li, Pharmacokinetics and treatment efficacy of camptothecin nanocrystals on lung metastasis, Mol. Pharm. 11 (1) (2014) 226–233.
[89] H. Zhang, C.P. Hollis, Q. Zhang, T. Li, Preparation and antitumor study of camptothecin nanocrystals, Int. J. Pharm. 415 (1–2) (2011) 293–300.
[90] D.M. Mudie, K. Murray, C.L. Hoad, S.E. Pritchard, M.C. Garnett, G.L. Amidon, P.A. Gowland, R.C. Spiller, G.E. Amidon, L. Marciani, Quantification of gastrointestinal liquid volumes and distribution following a 240 mL dose of water in the fasted state, Mol. Pharm. 11 (9) (2014) 3039–3047.
[91] D.M. Mudie, G.L. Amidon, G.E. Amidon, Physiological parameters for oral delivery and in vitro testing, Mol. Pharm. 7 (5) (2010) 1388–1405.
[92] S.C. Sutton, Role of physiological intestinal water in oral absorption, AAPS J. 11 (2) (2009) 277–285.
[93] C.P. Hollis, R. Zhao, T. Li, Hybrid nanocrystal as a versatile platform for cancer theranostics, in: K. Park (Ed.), Biomaterials for Cancer Therapeutics: Diagnosis, Prevention and Therapy, Woodhead Publishing, Cambridge 2013, pp. 186–204.
[94] B. Kahr, R.W. Gurney, Dyeing crystals, Chem. Rev. 101 (4) (2001) 893–951.
[95] J.E. Rayahin, J.S. Buhrman, R.A. Gemeinhart, Hybrid nanocrystals: university of Kentucky US20060280680A1, Expert. Opin. Ther. Pat. 22 (3) (2012) 341–348.
[96] H.C. Wang, M. Kurimoto, B. Kahr, J. Chmielewski, α-Lactose monohydrate single crystals as hosts for matrix isolation of guest biopolymers, Bioorgan. Med. Chem. 9 (9) (2001) 2279–2283.
[97] B. Marzec, D.C. Green, M.A. Holden, A.S. Coté, J. Ihli, S. Khalid, A. Kulak, D. Walker, C. Tang, D.M. Duffy, Y.-Y. Kim, F.C. Meldrum, Amino acid assisted incorporation of dye molecules within calcite crystals, Angew. Chemie Int. Ed. 57 (28) (2018) 8623–8628.
[98] D.C. Green, J. Ihli, P.D. Thornton, M.A. Holden, B. Marzec, Y.Y. Kim, A.N. Kulak, M.A. Levenstein, C. Tang, C. Lynch, S.E. Webb, C.J. Tynan, F.C. Meldrum, 3D visualization of additive occlusion and tunable full-spectrum fluorescence in calcite, Nat. Commun. 7 (2016) 13524.
[99] D. Xia, J. Tao, Y. He, Q. Zhu, D. Chen, M. Yu, F. Cui, Y. Gan, Enhanced transport of nanocage stabilized pure nanodrug across intestinal epithelial barrier mimicking listeria monocytogenes, Biomaterials 37 (2015) 320–332.
[100] Z. Lin, D. Mei, M. Chen, Y. Wang, X. Chen, Z. Wang, B. He, H. Zhang, X. Wang, W. Dai, Y. Yin, Q. Zhang, A comparative study of thermo-sensitive hydrogels with water-

insoluble paclitaxel in molecule, nanocrystal and microcrystal dispersions, Nanoscale 7 (36) (2015) 14838–14847.
[101] H. Hu, Z. Lin, B. He, W. Dai, X. Wang, J. Wang, X. Zhang, H. Zhang, Q. Zhang, A novel localized co-delivery system with lapatinib microparticles and paclitaxel nanoparticles in a peritumorally injectable in situ hydrogel, J. Control. Release 220 (Pt A) (2015) 189–200.
[102] D. Ni, H. Ding, S. Liu, H. Yue, Y. Bao, Z. Wang, Z. Su, W. Wei, G. Ma, Superior intratumoral penetration of paclitaxel nanodots strengthens tumor restriction and metastasis prevention, Small 11 (21) (2015) 2518–2526.
[103] Y. He, D.N. Xia, Q.X. Li, J.S. Tao, Y. Gan, C. Wang, Enhancement of cellular uptake, transport and oral absorption of protease inhibitor saquinavir by nanocrystal formulation, Acta Pharmacol. Sin. 36 (9) (2015) 1151–1160.
[104] T. Chen, C. Li, Y. Li, X. Yi, S.M. Lee, Y. Zheng, Oral delivery of a nanocrystal formulation of schisantherin a with improved bioavailability and brain delivery for the treatment of Parkinson's disease, Mol. Pharm. 13 (11) (2016) 3864–3875.
[105] W.C. Zamboni, J. Szebeni, S.V. Kozlov, A.T. Lucas, J.A. Piscitelli, M.A. Dobrovolskaia, Animal models for analysis of immunological responses to nanomaterials: challenges and considerations, Adv. Drug Deliv. Rev. 136-137 (2018) 82–96.
[106] Q. Dai, N. Bertleff-Zieschang, J.A. Braunger, M. Bjornmalm, C. Cortez-Jugo, F. Caruso, Particle targeting in complex biological media, Adv. Healthc. Mater. 7 (1) (2018).
[107] X. Hu, X. Dong, Y. Lu, J. Qi, W. Zhao, W. Wu, Bioimaging of nanoparticles: the crucial role of discriminating nanoparticles from free probes, Drug Discov. Today 22 (2) (2017) 382–387.
[108] Y. Hong, J.W. Lam, B.Z. Tang, Aggregation-induced emission, Chem. Soc. Rev. 40 (11) (2011) 5361–5388.
[109] J. Luo, Z. Xie, J.W. Lam, L. Cheng, H. Chen, C. Qiu, H.S. Kwok, X. Zhan, Y. Liu, D. Zhu, B.Z. Tang, Aggregation-induced emission of 1-methyl-1,2,3,4,5-pentaphenylsilole, Chem. Commun. 18 (2001) 1740–1741.
[110] S. Chen, H. Wang, Y. Hong, B.Z. Tang, Fabrication of fluorescent nanoparticles based on AIE luminogens (AIE dots) and their applications in bioimaging, Mater. Horiz. 3 (4) (2016) 283–293.
[111] X. Hu, W. Fan, Z. Yu, Y. Lu, J. Qi, J. Zhang, X. Dong, W. Zhao, W. Wu, Evidence does not support absorption of intact solid lipid nanoparticles via oral delivery, Nanoscale 8 (13) (2016) 7024–7035.
[112] Y.C. Xie, X.W. Hu, H.S. He, F. Xia, Y.H. Ma, J.P. Qi, X.C. Dong, W.L. Zhao, Y. Lu, W. Wu, Tracking translocation of glucan microparticles targeting M cells: implications for oral drug delivery, J. Mater. Chem. B 4 (17) (2016) 2864–2873.
[113] E. Ahmad, Y. Feng, J. Qi, W. Fan, Y. Ma, H. He, F. Xia, X. Dong, W. Zhao, Y. Lu, W. Wu, Evidence of nose-to-brain delivery of nanoemulsions: cargoes but not vehicles, Nanoscale 9 (3) (2017) 1174–1183.
[114] Y. Ma, H. He, F. Xia, Y. Li, Y. Lu, D. Chen, J. Qi, Y. Lu, W. Zhang, W. Wu, In vivo fate of lipid-silybin conjugate nanoparticles: implications on enhanced oral bioavailability, Nanomedicine 13 (8) (2017) 2643–2654.
[115] R. Su, W. Fan, Q. Yu, X. Dong, J. Qi, Q. Zhu, W. Zhao, W. Wu, Z. Chen, Y. Li, Y. Lu, Size-dependent penetration of nanoemulsions into epidermis and hair follicles: implications for transdermal delivery and immunization, Oncotarget 8 (24) (2017) 38214–38226.
[116] B. Wan, Y. Dai, D. Liu, J. Qi, X. Dong, W. Zhao, W. Wu, Y. Lu, Intraocular fate of polycaprolactone nanoparticles administered via intravitreal and various periocular routes: bioimaging of integral nanoparticles using environment-sensitive fluorophores, J. Biomed. Nanotechnol. 13 (8) (2017) 960–972.
[117] F. Xia, W. Fan, S. Jiang, Y. Ma, Y. Lu, J. Qi, E. Ahmad, X. Dong, W. Zhao, W. Wu, Size-dependent translocation of nanoemulsions via oral delivery, ACS Appl. Mater. Interfaces 9 (26) (2017) 21660–21672.
[118] H. He, S. Jiang, Y. Xie, Y. Lu, J. Qi, X. Dong, W. Zhao, Z. Yin, W. Wu, Reassessment of long circulation via monitoring of integral polymeric nanoparticles justifies a more accurate understanding, Nanoscale Horiz. 3 (2018) 397–407.
[119] D. Liu, B. Wan, J. Qi, X. Dong, W. Zhao, W. Wu, Y. Dai, Y. Lu, Z. Chen, Permeation into but not across the cornea: Bioimaging of intact nanoemulsions and nanosuspensions using aggregation-caused quenching probes, Chinese. Chem. Lett. (2018) https://doi.org/10.1016/j.cclet.2018.1011.1015.
[120] H. He, Y. Xie, Y. Lv, J. Qi, X. Dong, W. Zhao, W. Wu, Y. Lu, Bioimaging of intact polycaprolactone nanoparticles using aggregation-caused quenching probes: size-dependent translocation via oral delivery, Adv. Healthc. Mater. 7 (22) (2018), e1800711.
[121] D.L. Liu, B. Wan, J.P. Qi, X.C. Dong, W.L. Zhao, W. Wu, Y.K. Dai, Y. Lu, Z.J. Chen, Permeation into but not across the cornea: bioimaging of intact nanoemulsions and nanosuspensions using aggregation-caused quenching probes, Chinese. Chem. Lett. 29 (12) (2018) 1834–1838.
[122] M.F. Yao, L.L. He, D.J. McClements, H. Xiao, Uptake of gold nanoparticles by intestinal epithelial cells: impact of particle size on their absorption, accumulation, and toxicity, J. Agr. Food Chem. 63 (36) (2015) 8044–8049.
[123] K.M. Williams, K. Gokulan, C.E. Cerniglia, S. Khare, Size and dose dependent effects of silver nanoparticle exposure on intestinal permeability in an in vitro model of the human gut epithelium, J. Nanobiotech. 14 (1) (2016) 62.
[124] E.A. Jares-Erijman, T.M. Jovin, FRET imaging, Nat. Biotechnol. 21 (11) (2003) 1387–1395.
[125] D.M. Charron, G. Zheng, Nanomedicine development guided by FRET imaging, Nano Today 18 (2018) 124–136.
[126] S.W. Morton, X. Zhao, M.A. Quadir, P.T. Hammond, FRET-enabled biological characterization of polymeric micelles, Biomaterials 35 (11) (2014) 3489–3496.
[127] Y. Wu, Y.P. Ho, Y. Mao, X. Wang, B. Yu, K.W. Leong, L.J. Lee, Uptake and intracellular fate of multifunctional nanoparticles: a comparison between lipoplexes and polyplexes via quantum dot mediated Forster resonance energy transfer, Mol. Pharm. 8 (5) (2011) 1662–1668.
[128] S. Zhao, W. Dai, B. He, J. Wang, Z. He, X. Zhang, Q. Zhang, Monitoring the transport of polymeric micelles across MDCK cell monolayer and exploring related mechanisms, J. Control. Release 158 (3) (2012) 413–423.
[129] E. Roger, J.C. Gimel, C. Bensley, A.S. Klymchenko, J.P. Benoit, Lipid nanocapsules maintain full integrity after crossing a human intestinal epithelium model, J. Control. Release 253 (2017) 11–18.
[130] K.J. Chen, Y.L. Chiu, Y.M. Chen, Y.C. Ho, H.W. Sung, Intracellularly monitoring/imaging the release of doxorubicin from pH-responsive nanoparticles using Forster resonance energy transfer, Biomaterials 32 (10) (2011) 2586–2592.
[131] A.L. Lainé, J. Gravier, M. Henry, L. Sancey, J. Béjaud, E. Pancani, M. Wiber, I. Texier, J.L. Coll, J.P. Benoit, C. Passirani, Conventional versus stealth lipid nanoparticles: formulation and in vivo fate prediction through FRET monitoring, J. Control. Release 188 (2014) 1–8.
[132] F. Cayre, S. Mura, B. Andreiuk, D. Sobot, S. Gouazou, D. Desmaele, A.S. Klymchenko, P. Couvreur, In vivo FRET imaging to predict the risk associated with hepatic accumulation of squalene-based prodrug nanoparticles, Adv. Healthc. Mater. 7 (3) (2018) 1700830.
[133] Y. Zhao, F. Fay, S. Hak, J. Manuel Perez-Aguilar, B.L. Sanchez-Gaytan, B. Goode, R. Duivenvoorden, C. de Lange Davies, A. Bjorkoy, H. Weinstein, Z.A. Fayad, C. Perez-Medina, W.J. Mulder, Augmenting drug-carrier compatibility improves tumour nanotherapy efficacy, Nat. Commun. 7 (2016) 11221.
[134] X. Sun, G. Wang, H. Zhang, S. Hu, X. Liu, J. Tang, Y. Shen, The blood clearance kinetics and pathway of polymeric micelles in cancer drug delivery, ACS Nano 12 (6) (2018) 6179–6192.
[135] K. Li, M. Yamamoto, S.J. Chan, M.Y. Chiam, W. Qin, P.T. Wong, E.K. Yim, B.Z. Tang, B. Liu, Organic nanoparticles with aggregation-induced emission for tracking bone marrow stromal cells in the rat ischemic stroke model, Chem. Commun. 50 (96) (2014) 15136–15139.
[136] Z. Zhao, B. Chen, J. Geng, Z. Chang, L. Aparicio-Ixta, H. Nie, C.C. Goh, L.G. Ng, A. Qin, G. Ramos-Ortiz, B. Liu, B.Z. Tang, Red emissive biocompatible nanoparticles from tetraphenylethene-decorated BODIPY luminogens for two-photon excited fluorescence cellular imaging and mouse brain blood vascular visualization, Part. Part. Syst. Charact. 31 (4) (2014) 481–491.
[137] D. Ding, R.T.K. Kwok, Y. Yuan, G. Feng, B.Z. Tang, B. Liu, A fluorescent light-up nanoparticle probe with aggregation-induced emission characteristics and tumor-acidity responsiveness for targeted imaging and selective suppression of cancer cells, Mater. Horiz. 2 (1) (2015) 100–105.
[138] D. Ding, K. Li, W. Qin, R. Zhan, Y. Hu, J. Liu, B.Z. Tang, B. Liu, Conjugated polymer amplified far-red/near-infrared fluorescence from nanoparticles with aggregation-induced emission characteristics for targeted in vivo imaging, Adv. Healthc. Mater. 2 (3) (2013) 500–507.
[139] J.R. Lakowicz, Principles of Fluorescence Spectroscopy, Springer, New York, USA, 2006.
[140] G. Feng, D. Mao, J. Liu, C.C. Goh, L.G. Ng, D. Kong, B.Z. Tang, B. Liu, Polymeric nanorods with aggregation-induced emission characteristics for enhanced cancer targeting and imaging, Nanoscale 10 (13) (2018) 5869–5874.
[141] N. Zhang, H. Chen, Y. Fan, L. Zhou, S. Trepout, J. Guo, M.-H. Li, Fluorescent polymersomes with aggregation-induced emission, ACS Nano 12 (4) (2018) 4025–4035.
[142] L. Yang, X. Wang, G. Zhang, X. Chen, G. Zhang, J. Jiang, Aggregation-induced intersystem crossing: a novel strategy for efficient molecular phosphorescence, Nanoscale 8 (40) (2016) 17422–17426.
[143] W. Wu, D. Mao, F. Hu, S. Xu, C. Chen, C.J. Zhang, X. Cheng, Y. Yuan, D. Ding, D. Kong, B. Liu, A highly efficient and photostable photosensitizer with near-infrared aggregation-induced emission for image-guided photodynamic anticancer therapy, Adv. Mater. 29 (33) (2017) 1700548.
[144] J. Qi, C. Sun, D. Li, H. Zhang, W. Yu, A. Zebibula, J.W.Y. Lam, W. Xi, L. Zhu, F. Cai, P. Wei, C. Zhu, R.T.K. Kwok, L.L. Streich, R. Prevedel, J. Qian, B.Z. Tang, Aggregation-induced emission luminogen with near-infrared-ii excitation and near-infrared-i emission for ultradeep intravital two-photon microscopy, ACS Nano 12 (8) (2018) 7936–7945.
[145] Z. Zheng, T. Zhang, H. Liu, Y. Chen, R.T.K. Kwok, C. Ma, P. Zhang, H.H.Y. Sung, I.D. Williams, J.W.Y. Lam, K.S. Wong, B.Z. Tang, Bright near-infrared aggregation-induced emission luminogens with strong two-photon absorption, excellent organelle specificity, and efficient photodynamic therapy potential, ACS Nano 12 (8) (2018) 8145–8159.
[146] R. Bouchaala, L. Mercier, B. Andreiuk, Y. Mély, T. Vandamme, N. Anton, J.G. Goetz, A.S. Klymchenko, Integrity of lipid nanocarriers in bloodstream and tumor quantified by near-infrared ratiometric FRET imaging in living mice, J. Control. Release 236 (2016) 57–67.
[147] C. Berney, G. Danuser, FRET or no FRET: a quantitative comparison, Biophys. J. 84 (6) (2003) 3992–4010.
[148] A. Roda, M. Guardigli, E. Michelini, M. Mirasoli, Nanobioanalytical luminescence: Förster-type energy transfer methods, Anal. Bioanal. Chem. 393 (1) (2008) 109.
[149] L. Gao, G. Liu, J. Ma, X. Wang, L. Zhou, X. Li, F. Wang, Application of drug nanocrystal technologies on oral drug delivery of poorly soluble drugs, Pharm. Res. 30 (2) (2013) 307–324.